A Failure Criterion to Explain the Test Specimen Thickness Effect on Fracture Toughness in the Transition Temperature Region

Elsevier Editorial System(tm) for Engineering Fracture Mechanics
Manuscript Draft

Manuscript Number: EFM-D-12-00366R1

Title: A Failure Criterion to Explain the Test Specimen Thickness Effect on Fracture Toughness in the Transition Temperature Region

Article Type: Research Paper

Keywords: Fracture mechanics; Constraint effect; Fracture toughness; Cleavage fracture; Transition temperature; Thickness effect; 3PB specimen.

Corresponding Author: Prof. Toshiyuki Meshii, PhD

Corresponding Author's Institution: University of Fukui

First Author: Toshiyuki Meshii, Dr. Engineering

Order of Authors: Toshiyuki Meshii, Dr. Engineering; Kai Lu, MS Engineering; Ryota Takamura, BS

Abstract: This paper considered the test specimen thickness (TST) effect on the fracture toughness of a material Jc in the transition temperature region for 3 point bending (3PB) specimens. Fracture toughness tests and elastic-plastic finite element analyses (FEA) with non-standard test specimens, which are non-standard because the specimen thickness-to-width ratio B/W was varied in the range of 0.25 to 1.5, were conducted. Based on these tests and the FEA results, it was demonstrated that the "planar" (4delta-t, sigma22c) failure criterion—which states that cleavage fracture after significant plastic deformation occurs when the crack opening stress sigma22 at a distance from the crack-tip that is equal to 4 times the crack-tip opening displacement delta-t exceeds a critical value sigma22c—was verified to effectively explain the TST effect. This (4delta-t, sigma22c) criterion also successfully predicted the tendency of Jc to saturate to some bounding value for B/W=1.0. This tendency was similar to that of the T33-stress, which is the out-of-plane elastic crack-tip constraint parameter. Because the (4delta-t, sigma22c) criterion could predict the TST effect on Jc and because the criterion could predict the bounded behavior of Jc for large B/W, the TST effect was concluded to be mainly mechanical in nature, which the weakest link model fails to predict. The mechanical cause of the TST effect on Jc was considered to be an out-of-plane crack-tip constraint, and one of its measures of magnitude is the T33-stress.

- The test specimen thickness (TST) effect on the fracture toughness J_c was considered.
- The TST effect on J_c and bounded behavior of J_c was observed with the non-standard 3PB specimen.
- A large-strain, elastic-plastic FEA reproduced the behaviors observed in the experiments.
- The ($4\delta_t$, σ_{22c}) failure criterion effectively explained the TST effect.
- The mechanical nature of the TST effect on J_c was demonstrated.

A Failure Criterion to Explain the Test Specimen Thickness Effect on Fracture Toughness in the Transition Temperature Region

Toshiyuki MESHII [a]*, Kai LU [b] and Ryota TAKAMURA[b]

[a] Faculty of Engineering, University of Fukui, 3-9-1 Bunkyo, Fukui, Fukui, JAPAN.

[b] Graduate Student, Graduate School of Engineering, University of Fukui, 3-9-1 Bunkyo, Fukui, Fukui, JAPAN.

*Correspondent, E-mail: meshii@u-fukui.ac.jp, FAX : +81-776-27-9764

Abstract

This paper considered the test specimen thickness (TST) effect on the fracture toughness of a material J_c in the transition temperature region for 3 point bending (3PB) specimens. Fracture toughness tests and elastic-plastic finite element analyses (FEA) with non-standard test specimens, which are non-standard because the specimen thickness-to-width ratio B/W was varied in the range of 0.25 to 1.5, were conducted. Based on these tests and the FEA results, it was demonstrated that the "planar" ($4\,\delta_t$, σ_{22c}) failure criterion—which states that cleavage fracture after significant plastic deformation occurs when the crack opening stress σ_{22} at a distance from the crack-tip that is equal to 4 times the crack-tip opening displacement δ_t exceeds a critical value σ_{22c}—was verified to effectively explain the TST effect. This ($4\delta_t$, σ_{22c}) criterion also successfully predicted the tendency of J_c to saturate to some bounding value for B/W=1.0. This tendency was similar to that of the T_{33}-stress, which is the out-of-plane elastic crack-tip constraint parameter. Because the ($4\delta_t$, σ_{22c}) criterion could predict the TST effect on J_c and because the criterion could predict the bounded behavior of J_c for large B/W, the TST effect was concluded to be mainly mechanical in nature, which the weakest link model fails to predict. The mechanical cause of the TST effect on J_c was considered to be an out-of-plane crack-tip constraint, and one of its measures of magnitude is the T_{33}-stress.

Key words: Fracture mechanics; Constraint effect, Fracture toughness, Cleavage fracture, Transition temperature, Thickness effect, 3PB specimen.

1. Introduction

One of the difficulties in determining the cleavage fracture toughness J_c of a material over the ductile-to-brittle transition (DBT) temperature region, which is important in the assessment of aging steel structures and reactor pressure vessels, is that test specimen thickness (TST) has an effect on J_c, even though standardized test specimens are used [1]. The two most physically logical effects, in general, are the statistically weakest link size effect and the loss of crack-tip constraint, that is, the effect caused by the loss of stress triaxiality [2]. The weakest link size effect should affect only brittle fracture, whereas the loss of constraint should affect both ductile and brittle fracture. Both criteria lead to increasing toughness with decreasing TST. Another point of view is that the former criterion considers the TST effect on J_c to be a material issue and the latter to be a mechanical issue.

This effect of TST on J_c, described as $J_c \propto B^{-1/2}$ ($B \equiv$ TST) by Wallin [2], was reproduced by Dodds et al. [3] based on the weakest link model. ASTM E1921 [4] has adopted parts of this criterion, and it seems to be widely accepted. However, as Dodds et al. [3] admit, "fracture toughness does not decrease indefinitely with thickness."

The crack-tip constraint approach to the TST effect on J_c assumes that the effect is a result of the out-of-plane crack-tip constraint. Guo [5, 6] proposed a parameter $T_z = \sigma_{33}/(\sigma_{11}+\sigma_{22})$ to measure the magnitude of the out-of-plane crack-tip constraint, and has been extensively working with co-workers to express the crack-tip stress field with a stress intensity factor (SIF) K or J-T_{11}-T_z [6-13]. Niemitz et al. [14] instead applied a J-Q-T_z approach to explain the difference in J_c. Whether explicitly expressed or not, Gao [15], Wang et al. [16-20], and Fernández-Sáez and Fernández-Canteli et al. [21] have focused their attention on the out-of-plane T-stress, T_{33}, as a measure of the out-of-plane crack-tip constraint. Based on this general methodology to express the magnitude of the 3D (including out-of-plane) crack-tip constraint, one of the authors [22] assumed that the TST effect on J_c was mechanical in nature and conducted fracture toughness tests and elastic-plastic finite element analyses (FEA) with non-standard compact-tension (CT) test specimens, using specimen thickness-to-width ratios, B/W, of 0.25, 0.4 and 0.5. The planar configuration was identical for the three cases and it complied with ASTM E399 [23] for W = 25 mm (these three types of test specimens are designated as non-standard test specimens). The key idea of this non-standard CT specimen was that the normalized planar parameter, $\beta_{11} = (\pi a)^{1/2}T_{11}/K$ (a = crack depth), is kept nearly constant, but the out-of-plane parameter, $\beta_{33} = (\pi a)^{1/2}T_{33}/K$, significantly changes for B/W. They successfully correlated the TST effect with a mechanical parameter as $J_c \propto |T_{33}|^{1/2}$ for 0.55% carbon steel JIS S55C in the DBT temperature region. The result was accepted as evidence that the TST effect on J_c is mechanical in nature, and the TST effect can be quantitatively described by some failure criterion independent of the specimen structure.

In this paper, as an extension of our previous work [22], the TST effect on J_c for a non-standard 3 point bending (3PB) specimen was studied to show that this effect is mechanical in nature. For this

purpose, fracture toughness tests with non-standard 3PB specimens were conducted for 0.55% carbon steel JIS S55C, and the TST effect was reproduced by running a large-strain, elastic-plastic FEA. Finally, it was demonstrated that the "planar" failure criterion proposed by Dodds et al. [24], i.e., that the "crack opening stress σ_{22c} together with the distance from the crack-tip which equals 4 times the crack-tip opening displacement δ_t," effectively explained the TST effect.

2. Fracture Toughness Test

2.1. Design of the non-standard 3PB specimens

It is well known that the widely accepted ASTM E1921 [4] (or E399 [23]) standard 3PB specimen (Fig. 1(a)) has a proportionally specified configuration based on its width W; i.e., the standard thickness-to-width ratio B/W is specified as 0.5 and the target crack depth-to-width ratio a/W is specified as 0.5. Under this specification, the normalized planar T-stress β_{11} (k = 1 in Eq. (1)) evaluated at the specimen mid-plane is approximately constant for W and, thus, for B. The starting point of our research was the recognition that if β_{11} represents the magnitude of the crack-tip constraint, then the TST effect on J_c observed for the standard 3PB specimens is independent of the crack-tip constraint. The volume of the specimen changes in proportion to B^3. When viewed in this manner, the explanation of the TST effect on J_c by the weakest link model, not by the loss of crack-tip constraint, is logical.

$$\beta_{kk} = T_{kk}\sqrt{\pi a}/K_{\mathrm{I}} \quad (k = 1 \text{or} 3)$$

where

$$\begin{Bmatrix} \sigma_{11} \\ \sigma_{22} \\ \sigma_{33} \\ \tau_{12} \\ \tau_{23} \\ \tau_{31} \end{Bmatrix} = \frac{K_{\mathrm{I}}}{\sqrt{2\pi r}} \begin{Bmatrix} \cos\frac{\theta}{2}\left(1-\sin\frac{\theta}{2}\sin\frac{3\theta}{2}\right) \\ \cos\frac{\theta}{2}\left(1+\sin\frac{\theta}{2}\sin\frac{3\theta}{2}\right) \\ 2\nu\cos\frac{\theta}{2} \\ \sin\frac{\theta}{2}\cos\frac{\theta}{2}\cos\frac{3\theta}{2} \\ 0 \\ 0 \end{Bmatrix} + \begin{Bmatrix} T_{11} \\ 0 \\ T_{33} \\ 0 \\ 0 \\ 0 \end{Bmatrix} \tag{1}$$

$$T_{33} = E\varepsilon_{33} + \nu T_{11} \tag{2}$$

The key idea in the design of the non-standard 3PB specimens for different Bs was to design the planar configuration to be in accordance with the ASTM E1921 (i.e., W = const.) but to change B/W to realize specimens with different thickness. With this design, it was expected that β_{11} would remain approximately constant but, because $|\varepsilon_{33}|$ in Eq. (2) decreases with increasing B, there would be a significant change in β_{33} at the specimen mid-plane where the cleavage fracture initiates. Here, E and ν in Eq. (2) are the material's Young's modulus and Poisson's ratio, respectively.

If β_{33} represents the out-of-plane crack-tip constraint and the TST effect on J_c (TST effect) is observed for this non-standard 3PB specimen, then the out-of-plane crack-tip constraint might be a candidate to explain the TST effect. If J_c shows a saturation tendency with increasing B for this non-standard 3PB specimen and β_{33} also shows a similar tendency for an identical B, then the TST effect is likely to be dominated by the out-of-plane crack-tip constraint.

In the following, an elastic FEA for the non-standard 3PB specimen with W = 25 mm (Fig. 3) was run for various B/Ws to determine B such that β_{33} at the specimen mid-plane saturated. The typical FEA model used in elastic analysis of the 3PB specimen is shown in Fig. 4. The crack length a was prescribed as $a/W = 0.5$ for all cases. One-quarter of the structure was analyzed, making use of symmetry (Fig. 4 (a)). Twenty-node hexahedral meshes were used. For all cases, the crack-tip was modeled by singular elements, whose size was Δl, and twenty equivalent rows of meshes were spaced inside the crack tube with radius R_s = 0.4 mm (Fig. 4 (b)). The details for the generated mesh are summarized in Table 1. The Young's modulus, E = 206 GPa, and Poisson's ratio, ν = 0.3, were used in all cases. WARP3D [25] was used as the FEA solver.

The SIF was evaluated by applying the domain integral method [26] to the FEA results. T_{11} was obtained by applying the domain integral [26] and interaction integral [27] methods to the FEA results. These methods for calculating various T_{11} solutions have been used widely in the past [12, 18-20]. T_{33} was evaluated from Eq. (2). The results at the specimen mid-plane are summarized in the normalized form as K/K_0, $\beta_{kk} = T_{kk}(\pi a)^{1/2}/K_0$ (k = 1, 3) in Fig. 5, in which K_0 is the nominal SIF calculated from the following equation in ASTM E1921 [4], corresponding to the load used for the calculation.

$$K = \frac{PS}{BW^{3/2}} f\left(\frac{a}{W}\right) \tag{3}$$

Here, $S = 4W$ is the support span, and f is a function of a/W that is given in the standard. Attention was focused upon the values at the mid-plane because the cleavage fracture is expected to initiate at the specimen mid-plane.

According to Fig. 5, the mid-plane K was not affected by B/W, as expected, and was close to the nominal 2D SIF K_0. The normalized T_{11}, where $\beta_{11} = T_{11}(\pi a)^{1/2}/K_0$, was positive, showing negligible dependence on B/W. The in-plane parameters at the specimen thickness center showed a slight dependence on B/W, as expected.

The dotted line represents $\nu\beta_{11}$, which denotes the case for $B/W \rightarrow \infty$ and $\varepsilon_{33} \rightarrow 0$, i.e., $T_{33} \rightarrow \nu T_{11}$ calculated from Eq. (2). The normalized T_{33}, where $\beta_{33} = T_{33}(\pi a)^{1/2}/K_0$, showed a strong dependence on B/W. β_{33} was negative for $B/W < 1.5$, very close to 0 for $B/W = 1.5$, positive for $B/W > 1.5$ and approached $\nu\beta_{11}$ with increasing B/W. Because a negative T-stress corresponds to a loss in crack-tip constraint [28], it appears that T_{33} represents the well-known tendency for a larger out-of-plane crack-tip constraint to be expected for thick test specimens. If β_{33} represents the

out-of-plane crack-tip constraint and if J_c has some bounding value for B due to the bounding nature of the crack-tip constraint for large B, deviation from the relationship $J_c \propto B^{-1/2}$ was expected to be observed for the non-standard 3PB specimen of $B/W \geq 1.5$. Because the magnitude of the positive T-stress is known to be insensitive to the crack-tip constraint [28] and because the load capacity of the testing machines is limited, fracture toughness tests for non-standard 3PB specimens with B/W = 0.25, 0.5, 1.0 and 1.5 were conducted.

2.2. Fracture toughness tests with the non-standard 3PB specimens

2.2.1. Material

The tested material was 0.55% carbon steel JIS S55C, which is known to be in the transition temperature region at room temperature. From the Charpy test results shown in Fig. 6, the fracture toughness test temperature was chosen to be 20 ^{o}C. The material was quenched at 850 ^{o}C and tempered at 650 ^{o}C. Chemical composition and mechanical properties of the heat-treated specimens are summarized in Tables 2 and 3, respectively. Two tensile tests were conducted in accordance with JIS Z2241 [29]. The loading rates of the tensile tests were 10 MPa/sec below 0.2% strain and 30 %/min (measured at the gage length) above 0.2%, which satisfies the JIS Z2241 [29] requirements of 3-30 MPa/sec below 0.2% strain and 20-50% /min (measured at the gage length) above 0.2%. The tensile test temperature was 20 ^{o}C.

2.2.2. Test specimens

As described in 2.1, the planar test specimen configurations were designed in accordance with ASTM E1921 [4] for width W = 25 mm, i.e., W was prescribed to be 25 mm for all specimens. In addition to the standard ASTM thickness-to-width ratio, B/W = 0.5, specimens with B/W = 0.25, 1.0, and 1.5 were prepared. After inserting a fatigue crack into the specimen, the crack length a satisfied ASTM's requirement of a/W = 0.45-0.55; the crack length was in the range of 0.49 to 0.51. Fatigue precrack was inserted at 20 ^{o}C with loads corresponding to K_{max} = 20 and 19 MPam$^{1/2}$ for the 1st and 2nd stages, respectively, which satisfied the requirement of the standard 25 and 20 MPam$^{1/2}$. Fatigue crack growth was monitored by clip gage. Five tests were conducted for each test specimen geometry.

2.2.3. Test results

The fracture toughness test was conducted in accordance with ASTM E1921 [4]. The loading rate was controlled to be 1.1 MPam$^{1/2}$/s, which is very small compared to the specification of ≤ 2.0 MPam$^{1/2}$/s. The test specimen temperature was maintained to be in the range of 20 ± 1 ^{o}C for 30/(25/B) minutes for B/W = 1.0 and 1.5, according to the standard. The hold time for the other cases of B/W = 0.25 and 0.5 was 30 minutes, which is longer than the standard hold time.

Typical fracture surfaces observed at the mid-plane for specimens of B/W = 0.25, 0.5 and 1.0 are shown in Fig. 8. It is clearly seen from Fig. 8 that cleavage fracture after plastic deformation was observed for all specimens with different B/Ws. Although not shown in this manuscript, a similar fractograph was observed for the case of B/W = 1.5. The difference observed in these three B/Ws was that the distance between the fatigue precrack and the river pattern decreased as B/W increased, corresponding to a decrease in the plastic zone.

Test results are summarized in Table 4 and Fig. 9. K_c in the table was obtained from Eq. (3) and is the SIF K corresponding to the maximum load, P_c. K_{Jc} in the table is the fracture toughness in terms of the SIF, defined as $K_{Jc} = [EJ_c/(1-\nu^2)]^{1/2}$, as specified in ASTM E1921 [4]. μ and Σ are the average and standard deviation of each value, respectively. $2\Sigma/\mu$ % is a reference value intended to represent the magnitude of data scatter.

It is seen from Table 4 that $2\Sigma/\mu$ of K_{Jc} were in the range of 20.7 to 39.9 % for all the specimens. Considering that the guideline for $2\Sigma/\mu$ given in ASTM E1921 for K_{Jc} is $56(1–20/\mu)$ % and was in the range of 45.0 to 49.5 % for the data in Table 4, it was concluded that the scatter in the K_{Jc} data summarized in the table is acceptable. In addition, if the datam for specimen number 1 with B/W = 0.5 is excluded, it can be said that a very small scatter in K_{Jc} was realized from the current test data.

One interesting fact was that the change in K_c, the SIF for the fracture load P_c, with B/W was very small, though a significant change in J_c was observed. The average K_c for each B/W was in the range of 61.1 to 64.0 MPam$^{1/2}$.

From Fig. 9, the TST effect on J_c was clearly observed for the non-standard 3PB specimens. The raw J_c tended to decrease as B/W increased in the range of 0.25 to 1.0 and seemed to saturate to a value around 46 N/mm for B/W = 1.5. If the relationship between the average values of J_c and B/W were fitted to $J_c \propto (B/W)^{-n}$, then n was large as 1 in the range of B/W = 0.25 to 0.5, decreased to 0.5 in the range of B/W = 0.5 to 1.0 and was almost 0 in range of B/W = 1.0 to 1.5; it was thus concluded that J_c was bounded for B/W = 1.5, on the point of the average of J_c.

In summary, by changing β_{33} for B/W of the non-standard 3PB, J_c displayed bounded behavior for large B and, thus, deviation from the relationship $J_c \propto B^{-1/2}$ was observed. This result was as expected under the assumptions that β_{33} represents the out-of-plane crack-tip constraint and that J_c is affected by this crack-tip constraint.

3. Failure Criterion to Account for the TST Effect on J_c

3. 1 Reproduction of the experiments with a large-strain, elastic-plastic FEA

First, a large-strain, elastic-plastic FEA for the non-standard 3PB test specimens was conducted to validate the assumption that the TST effect on J_c is mechanical in nature by reproducing the depicted experimental results without assuming the existence of micro-cracks in the material. After the assumption was validated, a failure criterion to explain the TST effect on J_c was proposed.

The FEA model used in the elastic-plastic analysis of the 3PB specimen is fundamentally similar with the model used for the elastic analysis shown in Fig. 4. The width W was 25 mm and the crack length a was 12.5 mm (a/W = 0.5) for all the models. One-quarter of the structure was analyzed to make use of the symmetry of the specimen as shown in Fig. 10(a). Twenty node hexahedral meshes were used. To run this large-strain elastic-plastic analysis, an initial blunted notch ρ was inserted at the crack-tip as shown in Fig. 10(b). Twenty rows of meshes were spaced around the notch and inside crack tube R_s = 0.8 mm. Equivalent elements were spaced in thickness direction. The details for the generated mesh are summarized in Table 5. In this case, ρ was validated by the relationship between the crack-tip opening displacement δ_t measured at node A in Fig. 10(b); in particular, δ_t/ρ was greater than 10. McMeeking and Parks [30] suggested that δ_t/ρ should be greater than 5 to ensure that the results would not be affected by the initial blunt notch. In addition, the FEA results were considered sufficiently accurate with very refined meshes because the blunted crack tip was always defined by fairly regularly spaced nodes and the region around a crack tip up to a distance of a few crack-tip openings was always composed of elements that were very small compared to δ_t.

WARP3D [25] was used for the large-strain, elastic-plastic analysis. The material behavior was assumed to be governed by the J2–incremental theory of plasticity, the isotropic hardening rule and the Prandtl–Reuss flow theory. The Newton–Raphson iterative method was used for the nonlinear convergence. The Young's modulus E = 206 GPa and Poisson's ratio ν = 0.3 were used for all cases. Because S55C is a material with yield drop, the total true stress-total true strain curve in the range up to the true fracture stress obtained from the two tensile tests was approximated as a piecewise-linear stress-strain curve, as shown in Fig. 11. Note that WARP3D [25] allows this kind of material modeling.

The maximum load for each B/W was selected as the average fracture load P_c obtained from the experiments, summarized in Table 4. Load P vs. crack-mouth opening displacement V_g curves (P-V diagrams) obtained from the FEA for each specimen type is compared with the experimental results in Fig. 12. J at the maximum load P_c was obtained from these FEA P-V diagrams in accordance with the ASTM E1921 [4] and designated as $J_{c\ FEA}$. This $J_{c\ FEA}$ was compared with the experimental results in Fig. 13.

It is seen in Fig. 12 that the large-strain, elastic-plastic FEA accurately reproduced the P-V diagrams observed from experiments, though a noticeable discrepancy was shown for the case B/W

= 0.25. The source of this discrepancy is examined in the Discussion. Although the fracture load P_c showed some scatter and the clip gage displacement at fracture also showed scatter, experimental P-V data for all the specimens were close to the curve drawn from the FEA results.

From Fig. 13, it is seen that $J_{c\ FEA}$ clearly reproduced the TST effect on J_c observed by the experiments. This was natural, because $J_{c\ FEA}$ was evaluated from the P-V diagrams that were confirmed to be fairly close to the experimental data. In addition, $J_{c\ FEA}$ displayed bounded behavior for large B.

In summary, by assuming the average fracture load P_c for each B/W of the non-standard 3PB specimens, J obtained from large strain FEA results at this P_c reproduced the TST effect on J_c observed from experiments. Because this large strain FEA did not assume existence of micro-cracks, but β_{33} was designed to be changed with the B/W of the non-standard 3PB specimens, TST effect on J_c seemed to be mechanical in nature, under the assumptions that β_{33} is to represent the out-of-plane crack-tip constraint.

3. 2 Failure criterion to explain the TST effect on J_c

If the TST effect on J_c is mechanical in nature, it was thought that a failure criterion applicable to large-strain, elastic-plastic FEA results that explains the TST effect on J_c might exist. The key idea for this criterion was that K_c, which is the SIF calculated from the fracture load P_c and the specimen size, was slightly dependent on TST, though J_c was significantly dependent, as shown in Table 4. The hypothesis was that the (in-plane) crack opening stress σ_{22} distribution for each specimen type at the critical load P_c may be similar, even though J_c shows noticeable effects from a change in B/W. This is because a change in B/W causes a negligible change in T_{11}. Thus, the "planar" failure criterion, similar to the one that Dodds et al. [24] applied to explain the J_c-dependence on the test specimen crack depth (as shown in Fig. 14), might be applied to explain the out-of-plane TST effect on J_c. The critical values of this criterion ($4\delta_t$, σ_{22c}), in which δ_t denotes the CTOD (crack-tip opening displacement) and σ_{22c} denotes the crack-opening stress, was evaluated as a first step.

The distribution of the crack opening stress σ_{22} ($\theta = 0$) at the specimen mid-plane ahead of the crack-tip with the fracture load P_c for all B/Ws are shown in Fig. 15. σ_{YS} in the figure is the true yield stress. σ_{22} ($\theta = 0$) for all B/Ws showed a similar tendency; specifically, σ_{22} attained a maximum value approximately equal to $5\sigma_{YS}$ at approximately $2\delta_t$. This maximum was comparable with that for a material with a hardening component of 5 at plane-strain, approximately equal to $5\sigma_{YS}$ [31].

The ($4\delta_t$, σ_{22c}) corresponding to the mid-plane $J_{c\ FEA}$ for each B/W calculated in 3.1 is summarized in Table 6. It is seen from Table 6 that the critical stress σ_{22c} at $4\delta_t$ on the crack plane ($\theta = 0$) was very close for all B/Ws in an engineering sense, though $J_{c\ FEA}$ for each B/W showed significant variation. The $J_{c\ FEA}$ at the mid-plane of the specimen was focused upon because cleavage fracture initiated at the specimen mid-plane. Because the σ_{22c} values for all the B/Ws were very close

at the fracture load for each P_c and J_{cFEA} at P_c reproduced the TST effect on J_c, it was concluded that the ($4\delta_t$, σ_{22c}) criterion successfully explained the TST effect on J_c.

In summary, the "planar" failure criterion ($4\delta_t$, σ_{22c}), which was applied to explain the crack depth dependence on J_c by Dodds et al. [24], successfully reproduced the TST effect on J_c that is observed in fracture toughness tests, under the assumption that the TST effect on J_c is mechanical in nature.

4. Discussion

In this work, the TST effect on J_c observed for 0.55% carbon steel S55C in the transition temperature range was reproduced by large-strain FEA results. Neither the micro-crack density distribution nor the weakest link model was assumed to apply to the material, as Dodds et al. did to deduce the relationship $J_c \propto B^{-1/2}$ [3]. The idea to change the crack-tip volume proportionally to the specimen thickness is common for non-standard specimens and the Dodds et al. framework. In addition, the "planar" failure criterion successfully explained the TST effect. Thus, it seems that the mechanical nature of the TST effect on J_c cannot be denied. At least, the bounded behavior of J_c with increasing B seems to be dominated by the mechanical nature. One of the candidates for this mechanical cause is the change in the out-of-plane crack-tip constraint. The only assumption applied in this study was that the fracture initiates at the specimen mid-plane.

In Fig. 12 (a), a noticeable discrepancy was shown for the P-V diagram of B/W = 0.25 obtained from both the experiments and FEA. The FEA was performed by assuming the crack length to be uniform in thickness direction and set as a/W = 0.5 (Fig. 10 (a)). However, after the fatigue pre-crack procedure, the crack length was, in fact, distributed along the thickness direction, especially for B/W = 0.25, as shown in Fig. 16 and Table 7. Thus, a large-strain, elastic-plastic FEA was performed for a case of B/W = 0.25, reflecting the fatigue crack length distribution for specimen id 4 as shown in Fig. 17.

The P-V diagram was compared with both the experiment and previous FEA results as shown in Fig. 18. It is seen from Fig. 18 that the P-V diagram from the FEA with a distributed length is closer to the experimental results. $J_{c\,FEA}$ obtained from the current P-V diagram increased to 90.3 N/mm, which corresponds to a 21.4 % increase from the uniform crack model 74.4 N/mm. This $J_{c\,FEA}$ for specimen id 4 became comparable to the minimum 93.4 N/mm of the experimental value, but is still smaller than the experimental result of 125.0 N/mm. Therefore, through-thickness crack length distribution was one noticeable source of discrepancy between J_{cFEA} and J_c for relatively thin specimens.

There might be an opinion that the quantity of the micro-cracks might have contributed in the discrepancy still remaining between $J_{c\,FEA}$ and J_c for this B /W. However, this discrepancy between $J_{c\,FEA}$ and J_c here is due to the discrepancy of P-V diagrams for FEA and experiments as shown in Fig. 18. Though not numerically verified, it seems difficult that the micro-crack density significantly affects a gross deformation, such as the P-V diagram. Therefore, the calculated J value from the P-V diagram seems also not to be significantly affected by micro-cracks.

5. Conclusions

This study investigated the TST effect on the fracture toughness J_c of a material in the transition temperature region for 3PB specimens. Fracture toughness tests and elastic-plastic FEA on non-standard test specimens, with thickness-to-width ratios B/W of 0.25, 0.5, 1.0 and 1.5, were conducted for 0.55% carbon steel. The conclusions are as follows.

- The TST effect on J_c and bounded behavior of J_c for increasing specimen B/W was observed with the non-standard 3PB specimen, as intended.
- Large-strain, elastic-plastic FEA reproduced the behavior observed in the experiments.
- The ($4\delta_t$, σ_{22c}) criterion effectively explained the TST effect and the bounded behavior of J_c.
- The bounded behavior of J_c for increasing B seems to be dominated by mechanical causes. One of the candidates for this mechanical cause is the change in out-of-plane crack-tip constraint.

Acknowledgement

Part of this work is supported by JSPS KAKENHI Grant Number 2456103. Their support is greatly appreciated.

List of figures

List of tables

References

[1] Petti JP, Dodds RH. Coupling of the Weibull stress model and macroscale models to predict cleavage fracture. Engineering Fracture Mechanics. 2004;71:2079-103.

[2] Wallin K. The size effect in K_{IC} results. Engineering Fracture Mechanics. 1985;22:149-63.

[3] Anderson TL, Stienstra D, Dodds RH. A Theoretical Framework for Addressing Fracture in the Ductile-Brittle Transition Region. In: Landes JD, McCabe DE, Boulet JAM, editors. STP1207, Fracture Mechanics: 24th Volume. Philadelphia: American Society for Testing and Materials; 1994. p. 186-214.

[4] ASTM. E1921-10 Standard Test Method for Determination of Reference Temperature, T_o, for Ferritic Steels in the Transition Range. Annual Book of ASTM Standards. Philadelphia PA: American Society for Testing and Materials; 2010.

[5] Guo W. Elastoplastic three dimensional crack border field--I. Singular structure of the field. Engineering Fracture Mechanics. 1993;46:93-104.

[6] Guo W. Elastoplastic three dimensional crack border field--II. Asymptotic solution for the field. Engineering Fracture Mechanics. 1993;46:105-13.

[7] Zhang B, Guo W. T_z constraints of semi-elliptical surface cracks in elastic plates subjected to uniform tension loading. International Journal of Fracture. 2005;131:173-87.

[8] Zhao J, Guo W, She C, Meng B. Three dimensional K-T_z stress fields around the embedded center elliptical crack front in elastic plates. Acta Mechanica Sinica. 2006;22:148-55.

[9] Zhao J, Guo W, She C. The in-plane and out-of-plane stress constraint factors and K-T-T_z description of stress fields near the border of a quarter-elliptical corner crack. Fatigue & Fracture of Engineering Materials & Structures. 2007;30:673-81.

[10] She C, Guo W. The out-of-plane constraint of mixed-mode cracks in thin elastic plates. International journal of solids and structures. 2007;44:3021-34.

[11] Zhang B, Guo W. Three-dimensional stress state around quarter-elliptical corner cracks in elastic plates subjected to uniform tension loading. Engineering Fracture Mechanics. 2007;74:386-98.

[12] Zhao J, Guo W, She C. The in-plane and out-of-plane stress constraint factors and K-T-T_z description of stress field near the border of a semi-elliptical surface crack. International Journal of Fatigue. 2007;29:435-43.

[13] Zhao J, Guo W, She C. Three-parameter approach for elastic-plastic fracture of the semi-elliptical surface crack under tension. International Journal of Mechanical Sciences. 2008;50:1168-82.

[14] Neimitz A, Galkiewicz J. Fracture toughness of structural components: influence of constraint. International Journal of Pressure Vessels and Piping. 2006;83:42-54.

[15] Gao H. Variation of elastic T-stresses along slightly wavy 3D crack fronts. International Journal of Fracture. 1992;58:241-57.

[16] Wang X. Elastic T-stress solutions for semi-elliptical surface cracks in finite thickness plates. Engineering Fracture Mechanics. 2003;70:731-56.

[17] Wang X. Elastic T-stress solutions for penny-shaped cracks under tension and bending. Engineering Fracture Mechanics. 2004;71:2283-98.

[18] Lewis T, Wang X. The T-stress solutions for through-wall circumferential cracks in cylinders subjected to general loading conditions. Engineering Fracture Mechanics. 2008;75:3206-25.

[19] Wang X, Bell R. Elastic T-stress solutions for semi-elliptical surface cracks in finite thickness plates subject to non-uniform stress distributions. Engineering Fracture Mechanics. 2004;71:1477-96.

[20] Qu J, Wang X. Solutions of T-stresses for quarter-elliptical corner cracks in finite thickness plates subject to tension and bending. International Journal of Pressure Vessels and Piping. 2006;83:593-606.

[21] González-Albuixech VF, Giner E, Fernández-Sáez J, Fernández-Canteli A. Influence of the T_{33}-stress on the 3-D stress state around corner cracks in an elastic plate. Engineering Fracture Mechanics. 2011;78:412-27.

[22] Meshii T, Tanaka T. Experimental T_{33}-stress formulation of test specimen thickness effect on fracture toughness in the transition temperature region. Engineering Fracture Mechanics. 2010;77:867-77.

[23] ASTM. E399-05 Standard Test Method for Plane-Strain Fracture Toughness of Metallic Materials. Annual Book of ASTM Standards. Philadelphia PA: American Society for Testing and Materials; 2005.

[24] Dodds RH, Anderson TL, Kirk MT. A framework to correlate a/W ratio effects on elastic-plastic fracture toughness (J_c). International Journal of Fracture. 1991;48:1-22.

[25] Gullerud A, Koppenhoefer K, Roy Y, RoyChowdhury S, Walters M, Bichon B, et al. WARP3D Release 15 Manual. Civil Engineering, Report No UIUCENG-95-2012, University of Illinois at Urbana-Champaign. 2004.

[26] Li FZ, Shih CF, Needleman A. A comparison of methods for calculating energy release rates. Engineering Fracture Mechanics. 1985;21:405-21.

[27] Nakamura T, Parks DM. Determination of elastic T-stress along three-dimensional crack fronts using an interaction integral. International journal of solids and structures. 1992;29:1597-611.

[28] Bilby BA, Cardew GE, Goldthorpe MR, Howard IC. A finite element investigation of the effect of specimen geometry on the fields of stress and strain at the tips of stationary cracks. Size Effects in Fracture. London: Mechanical Engineering Publications Limited; 1986. p. 37-46.

[29] JIS. Z2241 Method of tensile test for metallic materials. Tokyo: Japanese Industrial Standards Committee; 1998.

[30] McMeeking RM, Parks DM. On criteria for J-dominance of crack-tip fields in large-scale yielding. In: Landes John D, Begley JA, Clarke GA, editors. STP 668, Elastic-Plastic Fracture. Philadelphia, PA; USA: American Society for Testing and Materials; 1979. p. 120-38.

[31] McMeeking RM. Finite deformation analysis of crack-tip opening in elastic-plastic materials and implications for fracture. Journal of the Mechanics and Physics of Solids. 1977;25:357-81.

Nomenclature

B	Specimen thickness
E	Young's modulus
J	J-integral
J_c, $J_{c\ average}$	Fracture toughness and its average from experiments
$J_{c\ FEA}$	J obtained for fracture load P_c by FEA
K_I	Local mode-I stress intensity factor
K_{Jc}	Fracture toughness ($K_{Jc}= [EJ_c/(1-\nu^2)]^{1/2}$)
K_c	SIF corresponding to fracture load P_c
K_{max}	Maximum SIF in fatigue precracking procedure
K_0	Nominal SIF for elastic analysis
P, P_c	Applied and fracture load
R_s	Crack tube radius
S	Support span for 3PB specimen
T_{11}, T_{33}	T-stresses
V_g	Crack-mouth opening displacement
W	Specimen width
a	Crack length
n	Exponent
r, θ	In-plane polar coordinates
x_j	Crack-tip local coordinates (j = 1, 2, 3)
Δl	Singular element size
Σ	Standard deviation
β_{11}, β_{33}	Normalized T-stresses
δ_t	Crack-tip opening displacement
ε_{ij}	Strain components (i, j =1, 2, 3)
μ	Average value
ν	Poisson's ratio
ρ	Initial blunt notch radius
σ_{ij}	Stress components (i, j =1, 2, 3)
σ_{22c}	Critical crack opening stress
σ_{B0}	Tensile strength
σ_{YS} , σ_{YS0}	True and nominal yield stress

Table 1 Summary of the generated mesh for elastic analysis

(W = 25 mm, R_s = 0.4 mm, a/W = 0.5, $\Delta l/a$ = 0.0016)

B/W	0.25	0.4	0.5	0.75	1.0	1.25	1.5	1.6	1.7	1.8	1.9	2.0
na	15	20		25			30			35		
nodes	154197	203157		252117			301077			350037		
elements	35520	47360		59200			71040			82880		

Table 2 Chemical compositions of the test specimens in weight %

	C	Si	Mn	P	S	Cu	Ni	Cr	Fe
Specified	0.52~0.58	0.15~0.35	0.60~0.90	≤0.030	≤0.035	≤0.30	≤0.20	≤0.20	Balance
	0.55	0.17	0.61	0.015	0.004	0.13	0.07	0.08	Balance

Table 3 Mechanical properties of the test specimens

Yield Stress σ_{YS0} MPa	Tensile Strength σ_{B0} MPa	Elongation %
393, 394	703, 710	24.0, 23.3

Table 4 Fracture toughness test results for S55C

(3PB, W = 25 mm, 20 ^{o}C; μ: average, Σ: standard deviation)

B/W	Serial No.	1	2	3	4	5	μ	Σ	$2\mu/\Sigma$%
0.25	a/W	0.51	0.50	0.50	0.50	0.50	0.50	0.00	1.3
	P_c kN	5.39	6.26	5.29	5.99	6.17	5.82	0.45	15.4
	K_c MPa m$^{1/2}$	59.5	67.5	57.1	65.0	66.9	63.2	4.66	14.8
	J_c N/mm	93.4	152.9	106.7	125.0	197.9	135.2	41.6	61.5
	K_{Jc} MPa m$^{1/2}$	145.4	186.1	155.4	168.2	211.6	173.3	26.3	30.3
0.5	a/W	0.50	0.50	0.50	0.50	0.50	0.50	0.00	0.9
	P_c kN	10.5	12.0	10.8	11.6	11.4	11.3	0.61	10.8
	K_c MPa m$^{1/2}$	56.4	65.9	58.4	63.0	61.8	61.1	3.78	12.4
	J_c N/mm	30.5	93.6	50.9	70.6	67.7	62.7	23.5	75.2
	K_{Jc} MPa m$^{1/2}$	83.1	145.6	107.3	126.4	123.8	117.2	23.4	39.9
1.0	a/W		0.50	0.50	0.50	0.50	0.50	0.00	1.0
	P_c kN		22.7	22.4	24.1	23.8	23.2	0.84	7.3
	K_c MPa m$^{1/2}$		60.5	59.8	65.4	63.6	62.3	2.64	8.5
	J_c N/mm		35.9	33.5	61.1	55.8	46.6	13.9	59.8
	K_{Jc} MPa m$^{1/2}$		90.1	87.1	117.6	112.3	101.8	15.4	30.3
1.5	a/W	0.49		0.50	0.50	0.50	0.50	0.01	2.4
	P_c kN	34.9		35.7	37.3	35.0	35.7	1.09	6.1
	K_c MPa m$^{1/2}$	61.6		64.8	66.7	63.0	64.0	2.21	6.9
	J_c N/mm	37.1		46.7	59.3	41.0	46.0	9.68	42.1
	K_{Jc} MPa m$^{1/2}$	91.6		102.8	115.8	96.3	101.6	10.51	20.7

Table 5 Summary of the generated mesh for the elastic-plastic analysis
(W = 25 mm, R_s = 0.8 mm, a/W = 0.5)

B/W	ρ mm	na	N_theta	radial bias	nodes	elements
0.25	0.006	5	24	2	73876	15555
0.5	0.006	10	24	2	138146	31110
1.0	0.004	15	12	15	213652	49620
1.5	0.003	20	12	15	316632	74430

Table 6 Characteristic distance $4\delta_t$ and crack opening stress σ_{22c} at the fracture load P_c
(S55C, 3PB, W = 25 mm, a/W = 0.5)

B/W	0.25	0.5	1.0	1.5
K_c MPa $m^{1/2}$	63.2	61.1	62.3	64.0
$J_{c\ FEA}$ N/mm	74.5	45.0	34.3	36.7
$4\delta_t$ mm	0.34	0.22	0.15	0.15
σ_{22c} MPa	1480	1540	1510	1490

Table 7 Distributed crack length for $B/W = 0.25$ (specimen id 4)

a_1 mm	a_2 mm	a_3 mm	a_4 mm	a_5 mm	a_6 mm	a_7 mm	a_8 mm	a_9 mm
12.28	12.53	12.66	12.70	12.72	12.69	12.62	12.50	12.14

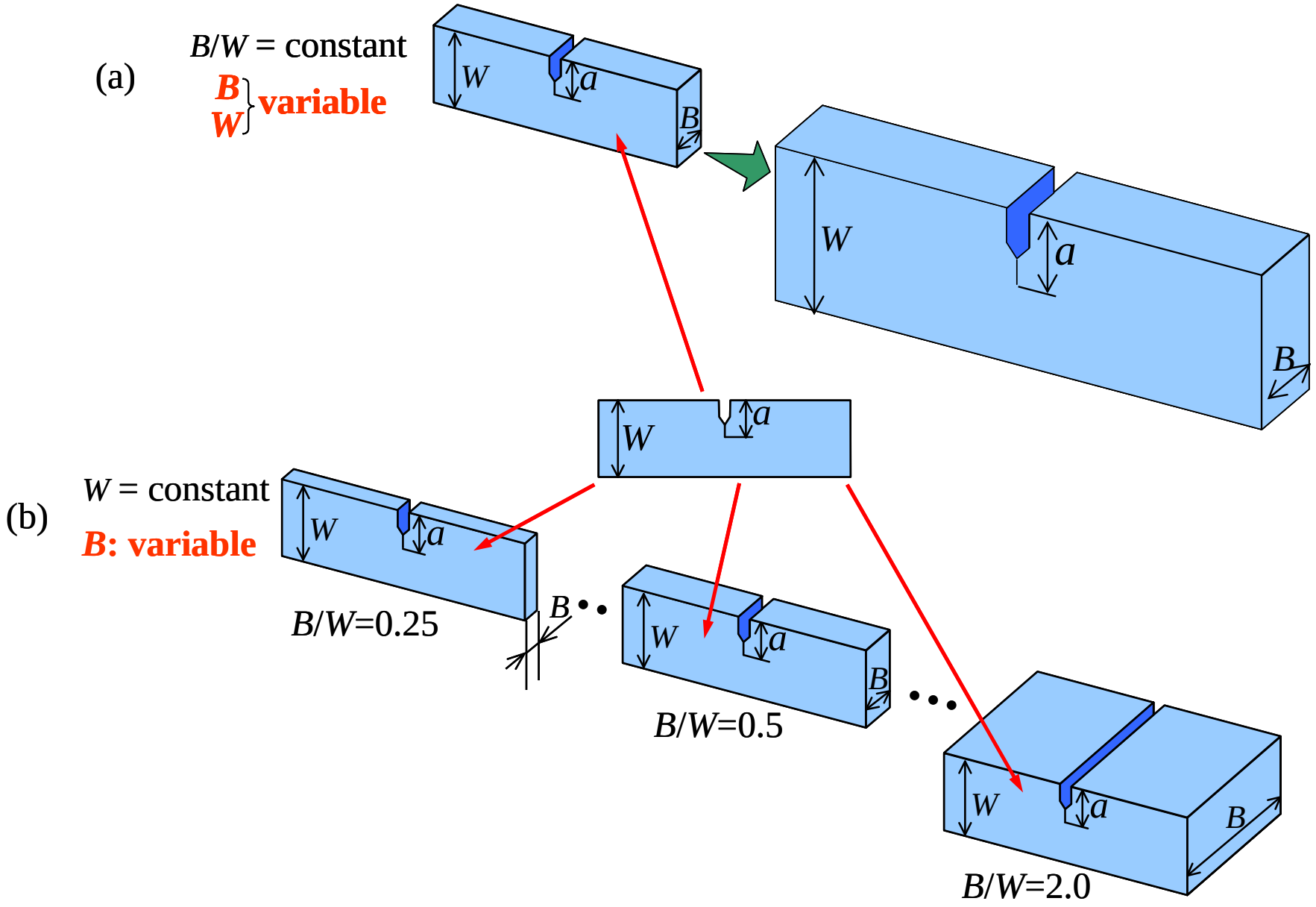

Fig. 1 (a) Standard and (b) non-standard 3PB specimens

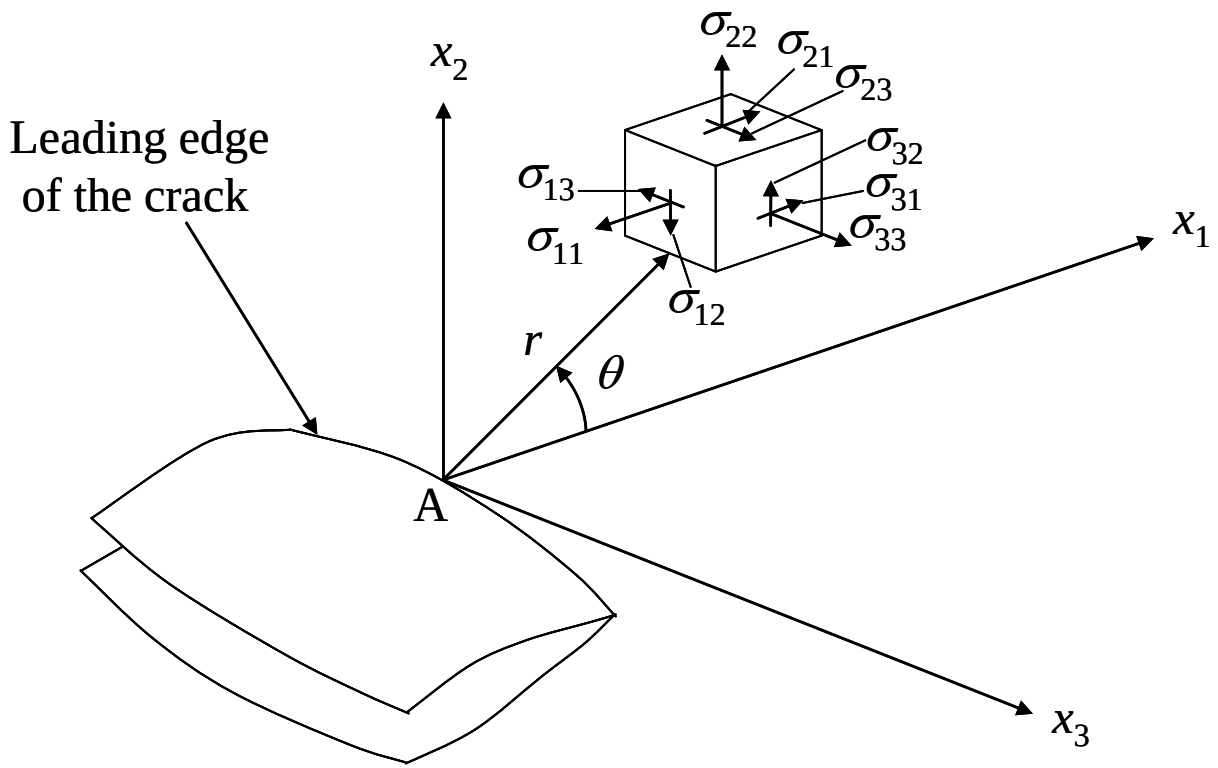

Fig. 2 Three-dimensional coordinate system for the region along the crack front

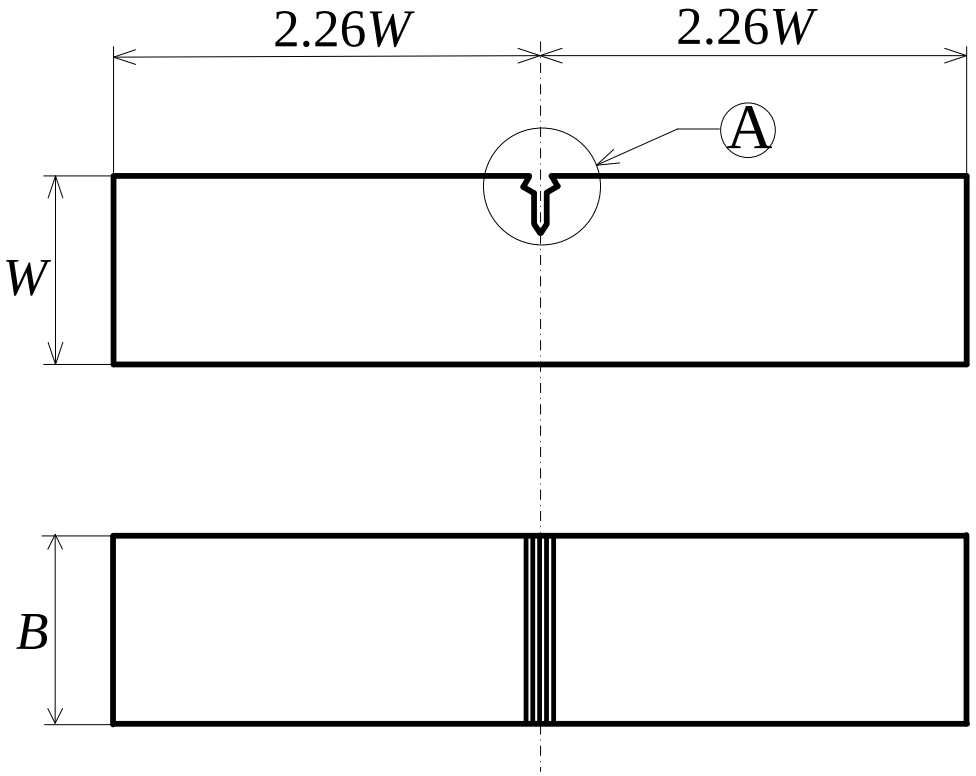

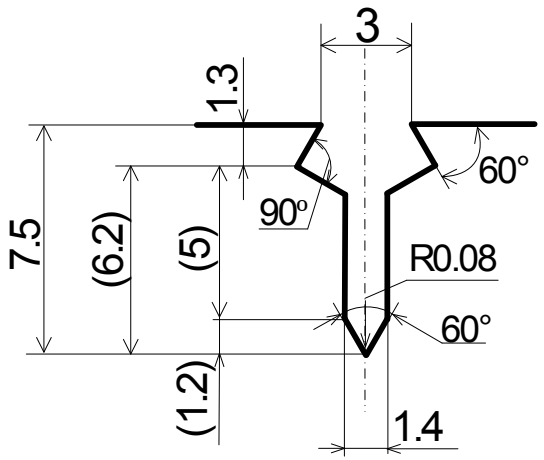

Detail of A (4□1□

Fig. 3 ASTM 3PB specimen

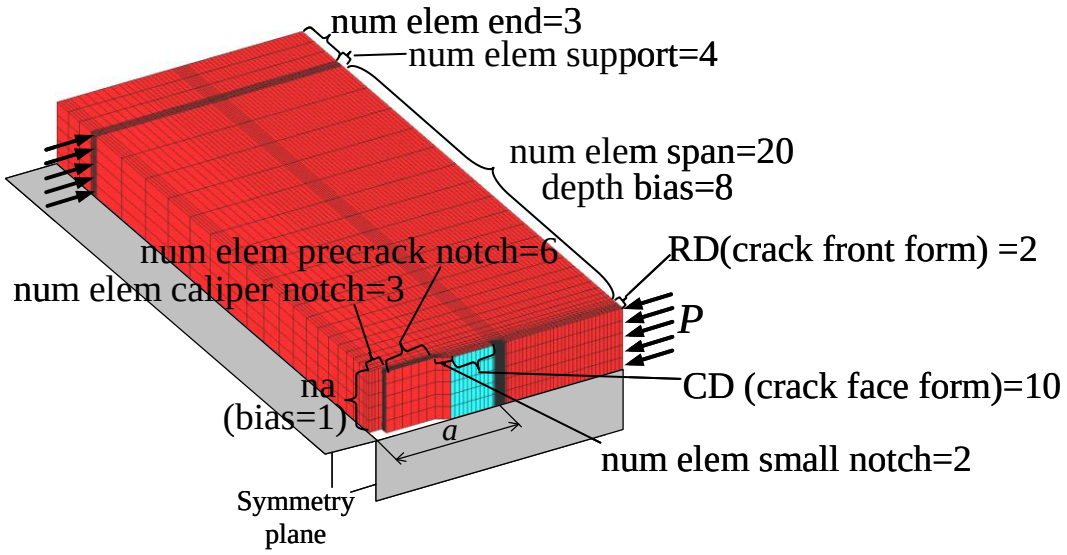

(a) Global mesh

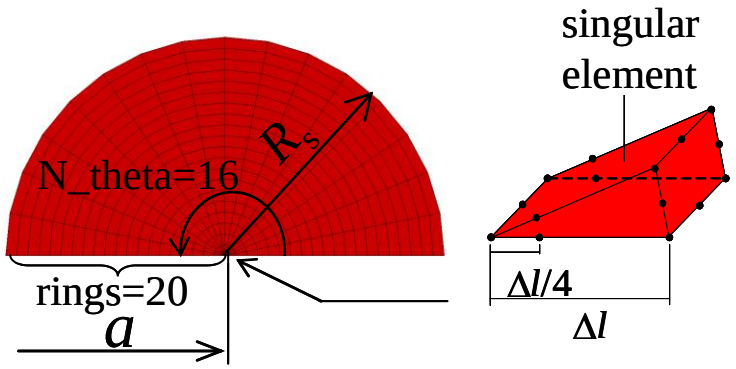

(b) Detail of crack tip
for elastic analysis

Fig. 4 Finite element model of 3PB specimen

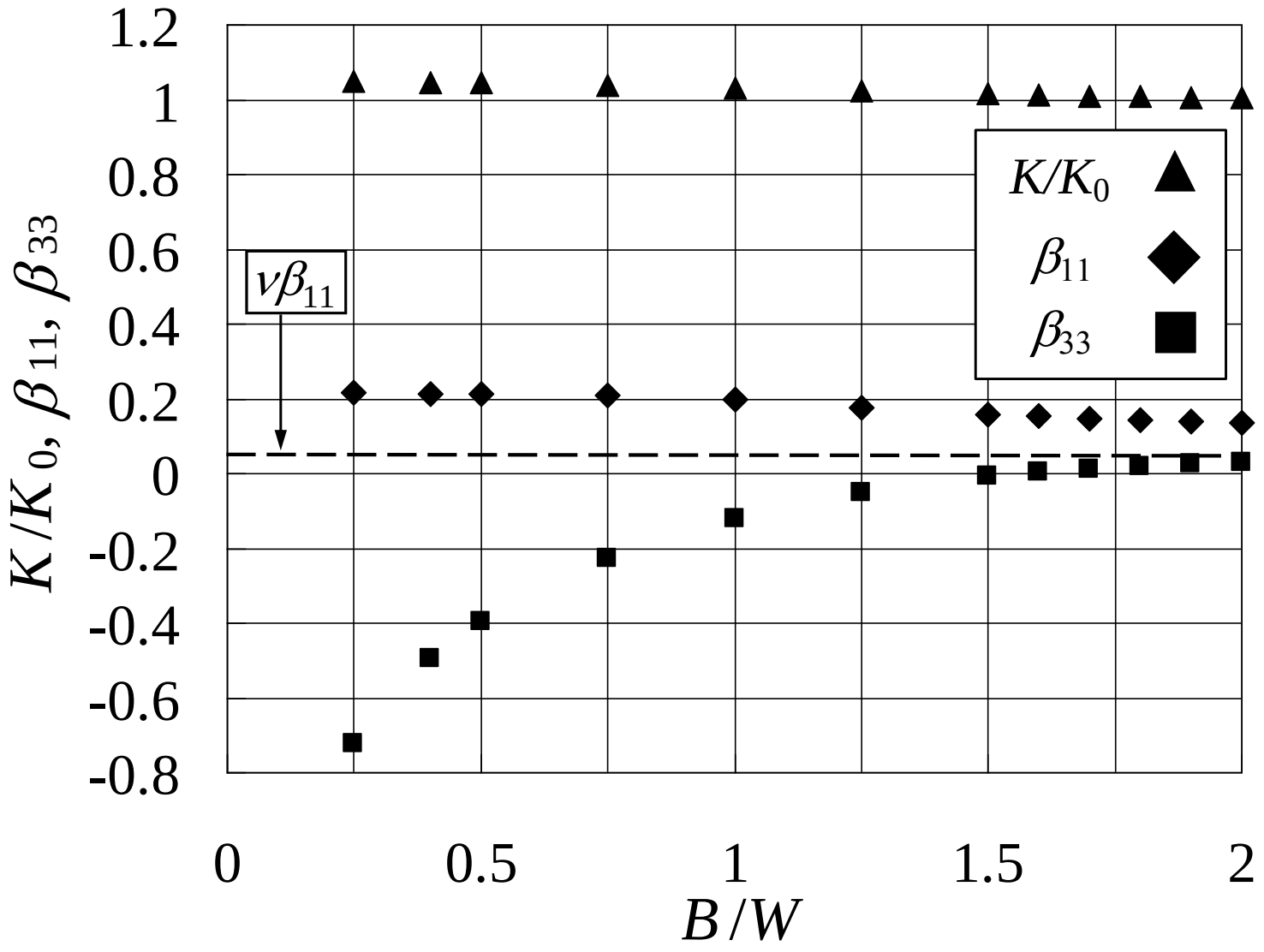

Fig. 5 The TST effect on normalized T_{11} and T_{33} of a non-standard 3PB specimen at the specimen mid-plane ($\nu = 0.3$)

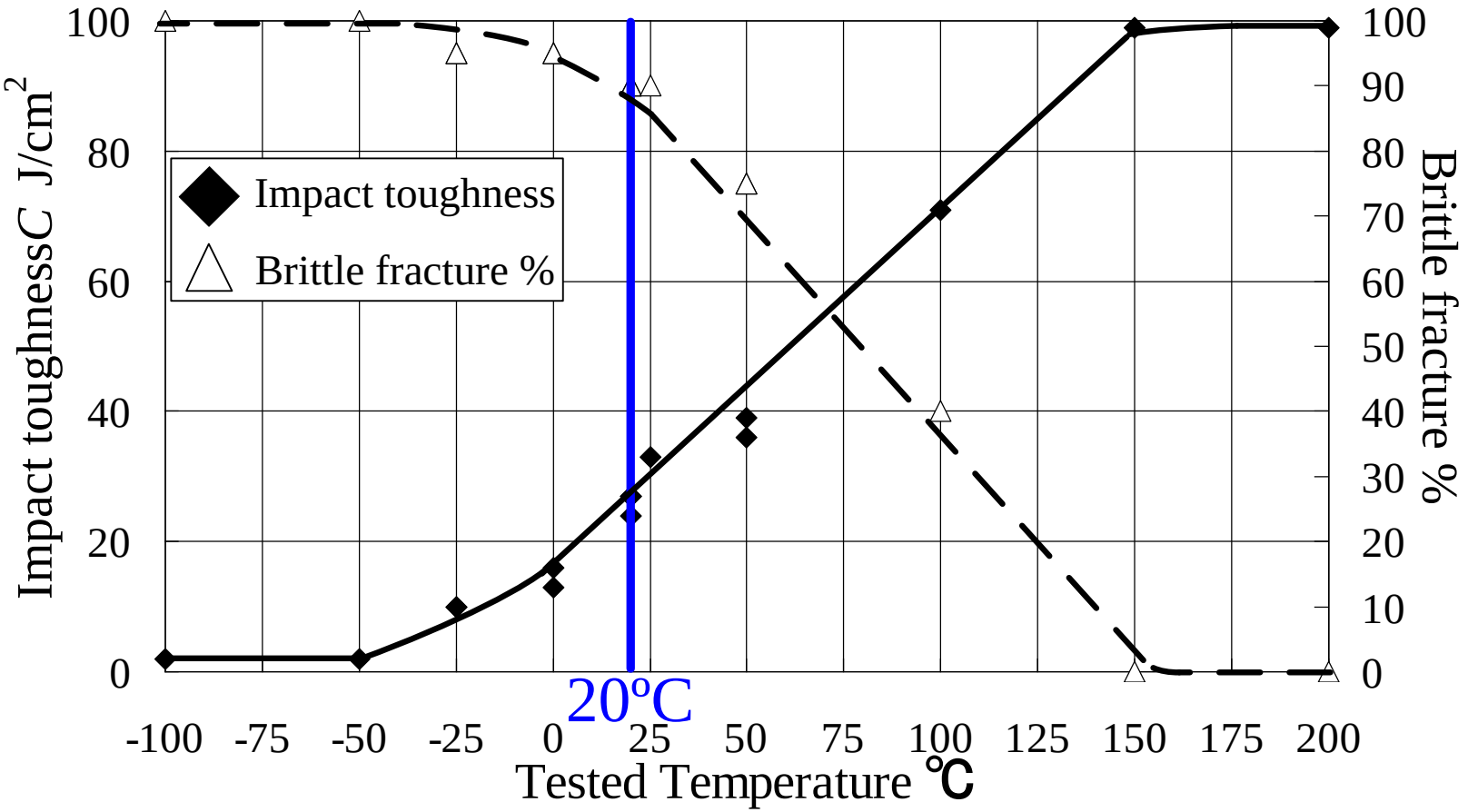

Fig. 6 Charpy test results for S55C

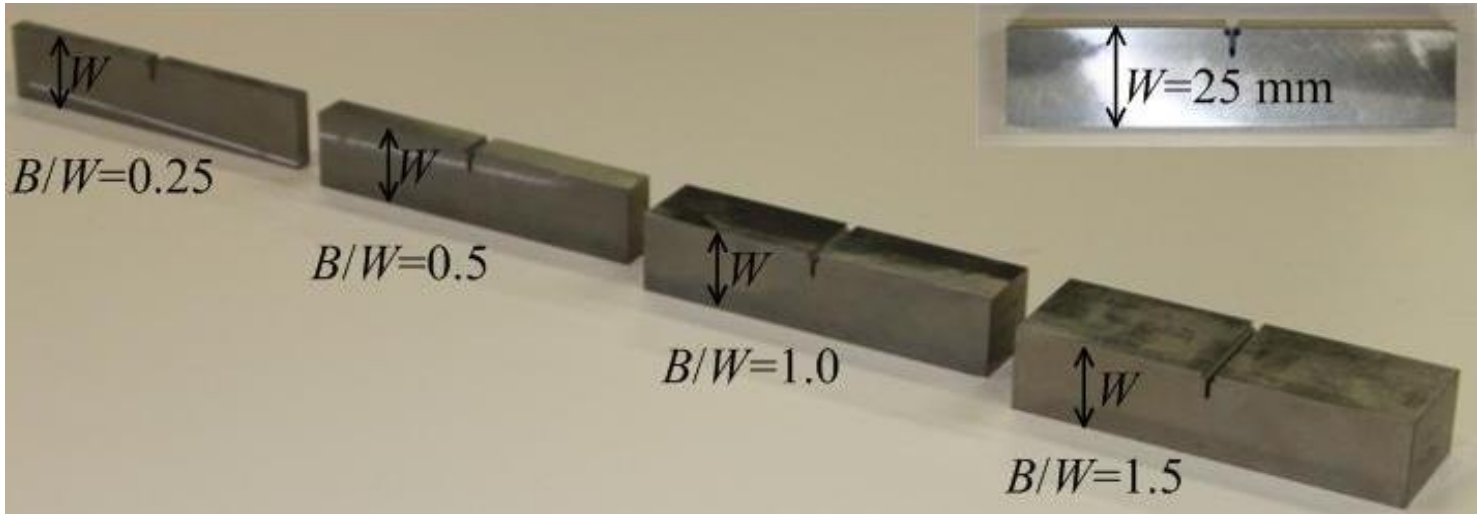

Fig. 7 Non-standard 3PB specimens

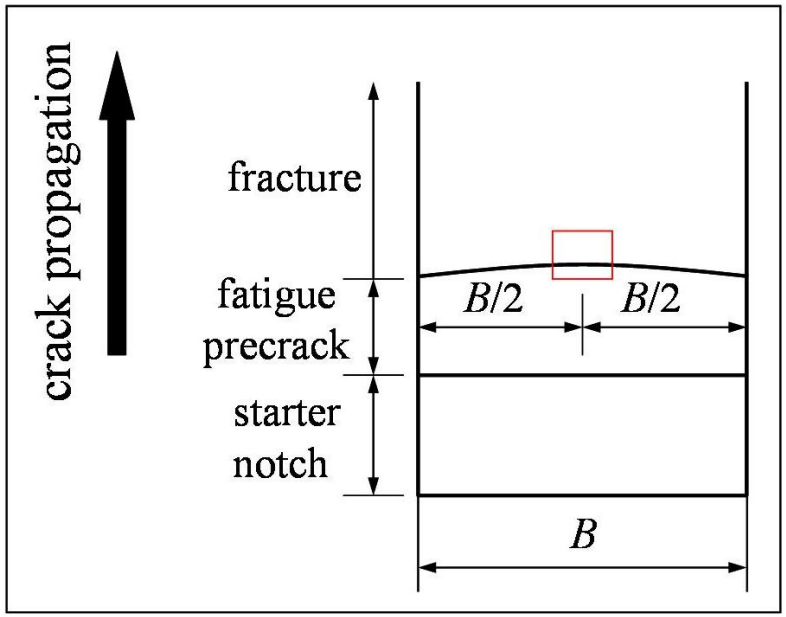

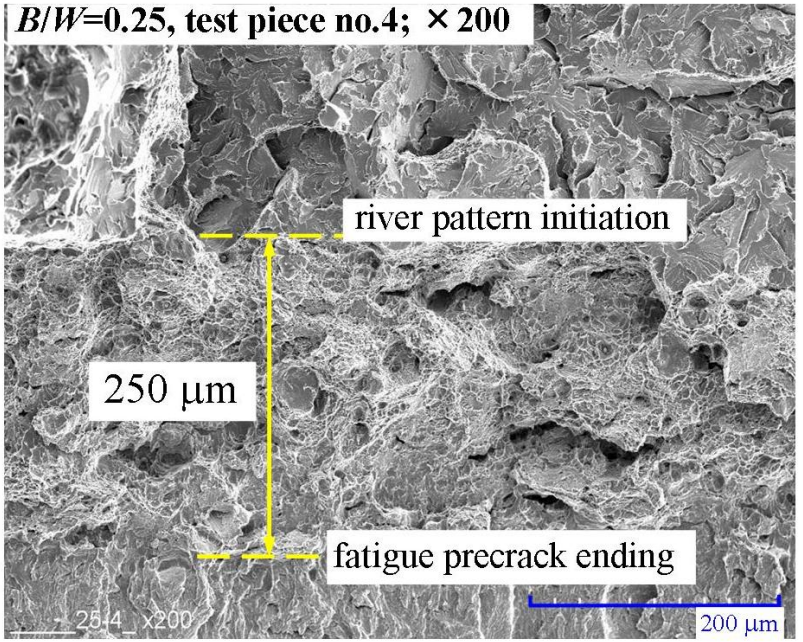

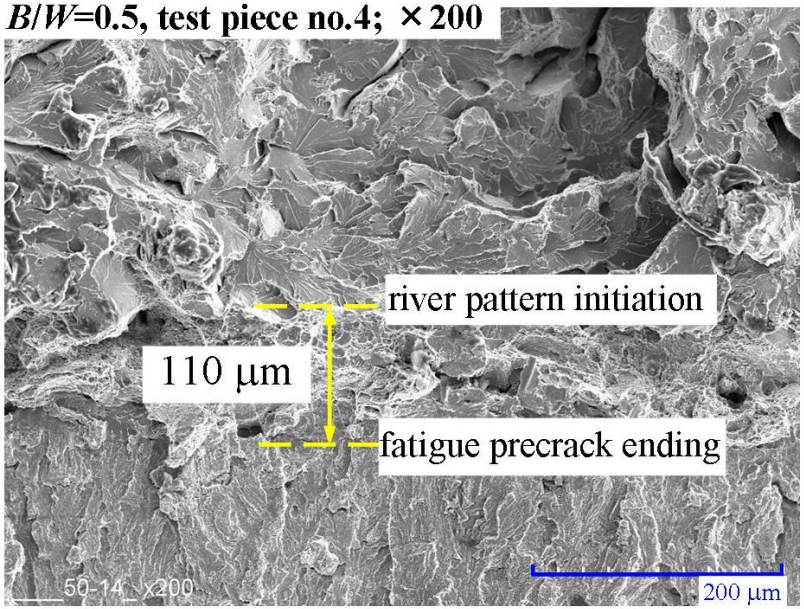

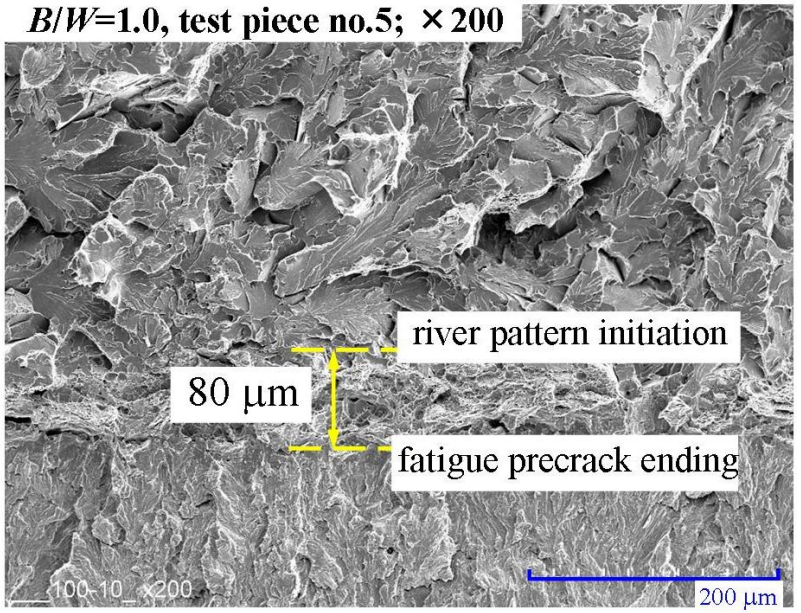

Fig. 8 Fracture surface of the specimens of B/W = 0.25, 0.5 and 1.0

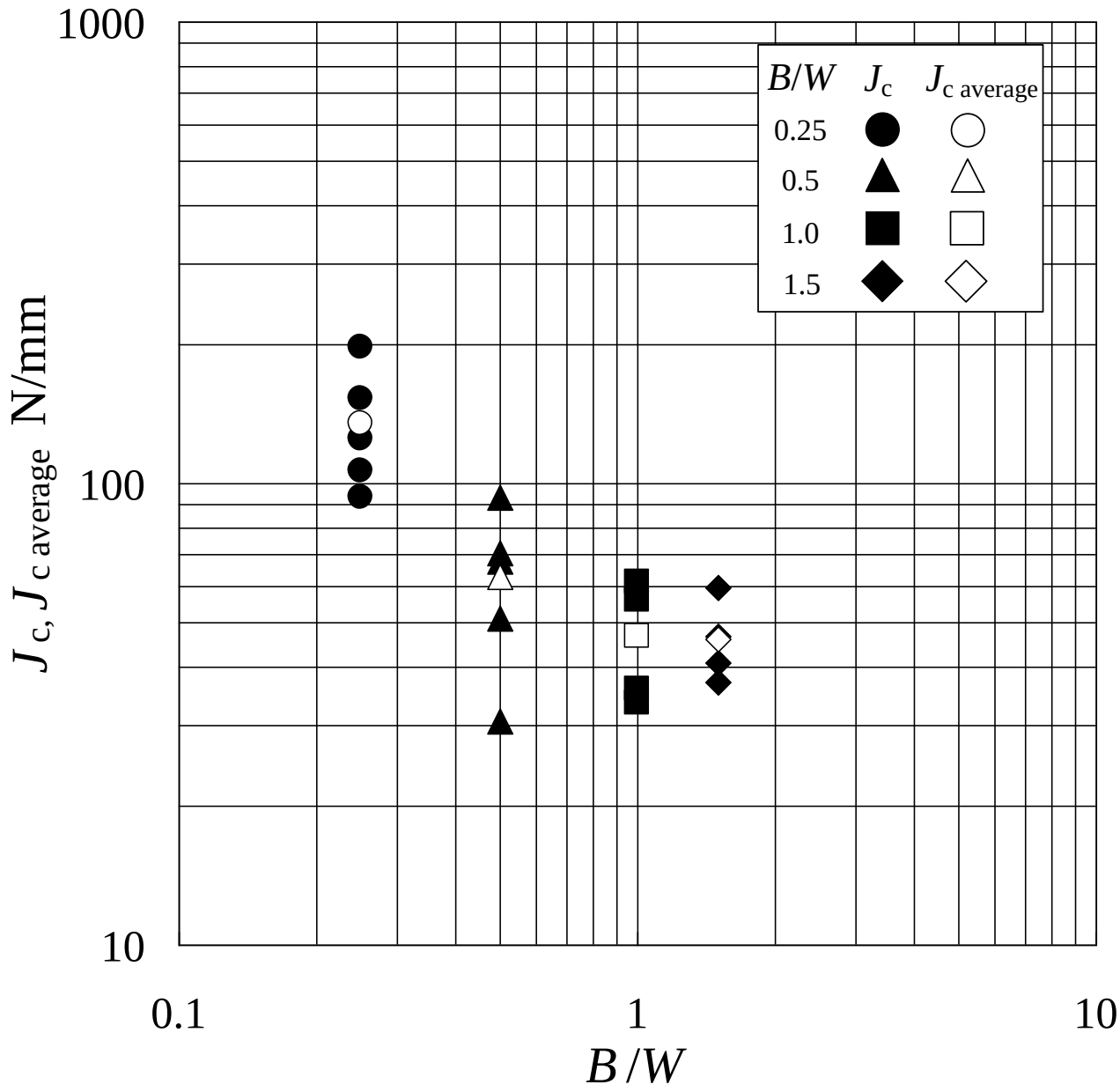

Fig. 9 Fracture toughness test results for the non-standard 3PB specimens (S55C, 20 ºC, W = 25 mm)

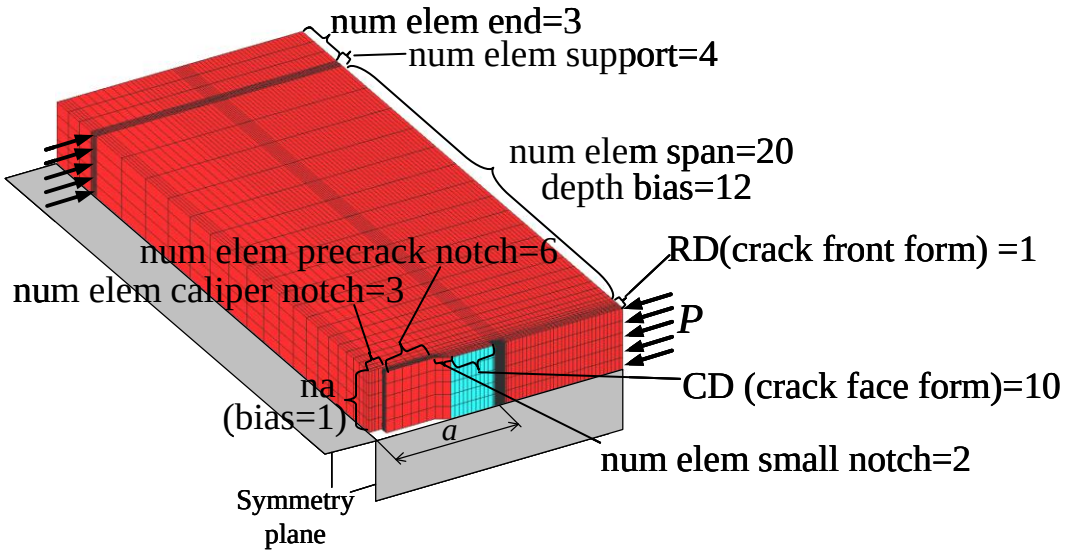

(a) Global mesh

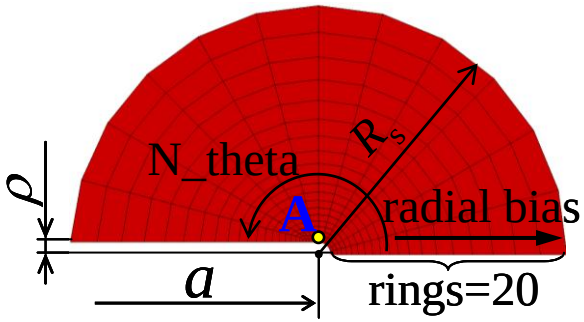

(b) Detail of crack tip for elastic-plastic analysis

Fig. 10 Large-strain, elastic-plastic FEA model

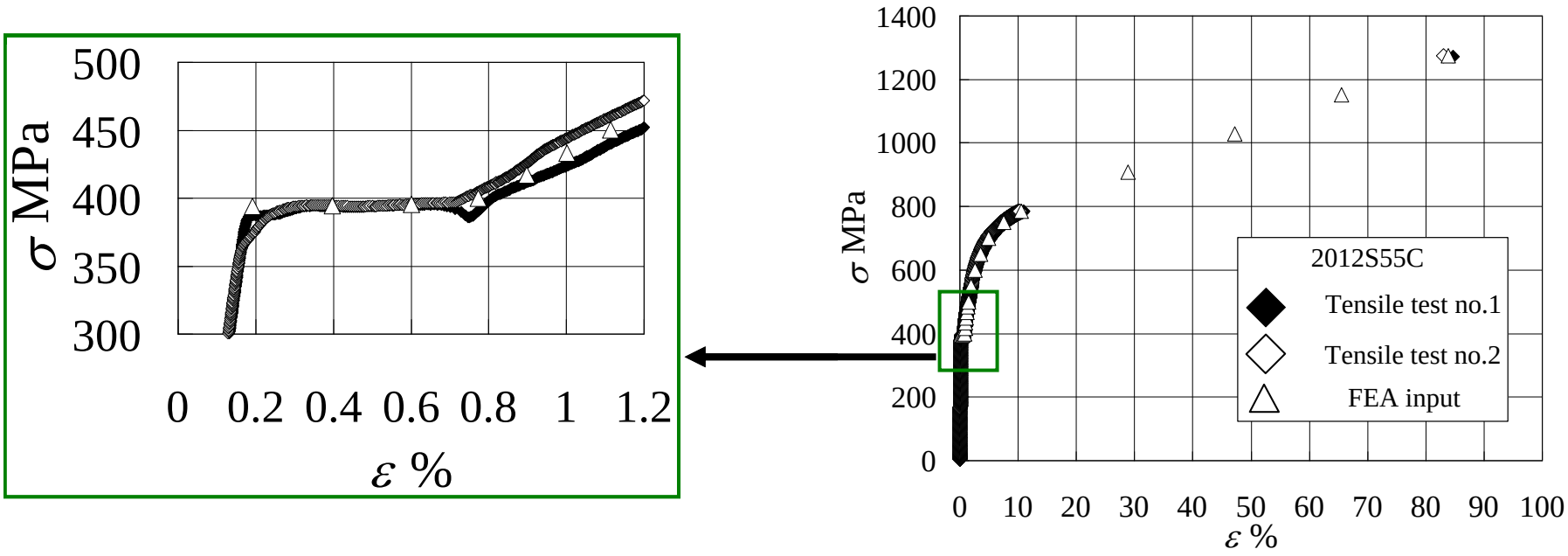

Fig. 11 Total true stress- total true strain curve for FEA (S55C)

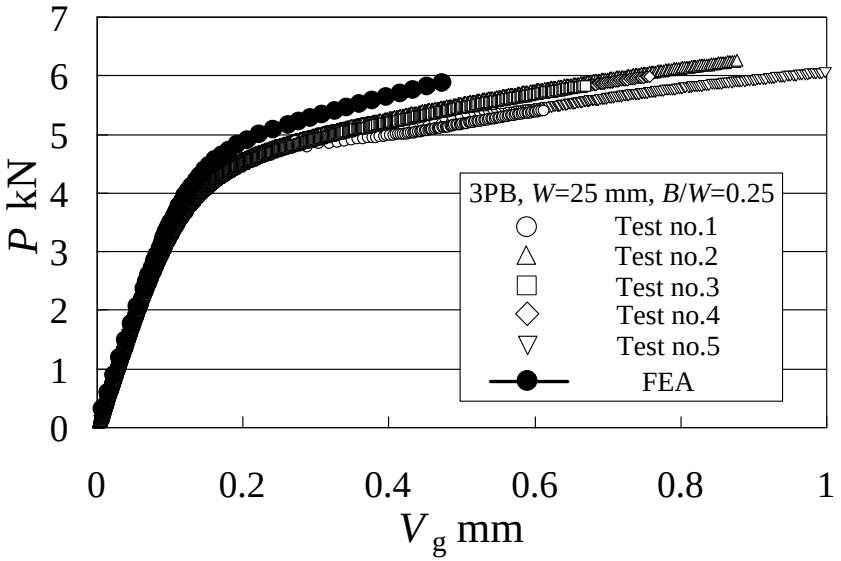

(a) $B/W = 0.25$

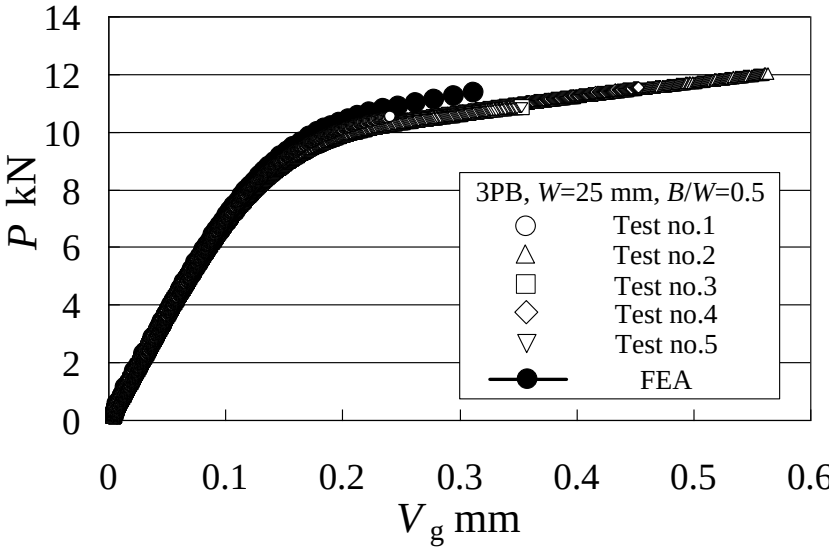

(b) $B/W = 0.5$

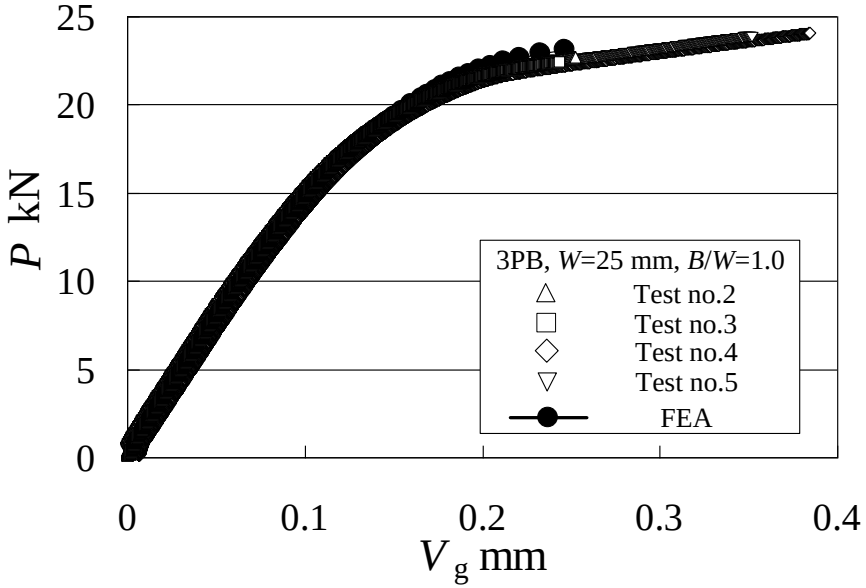

(c) $B/W = 1.0$

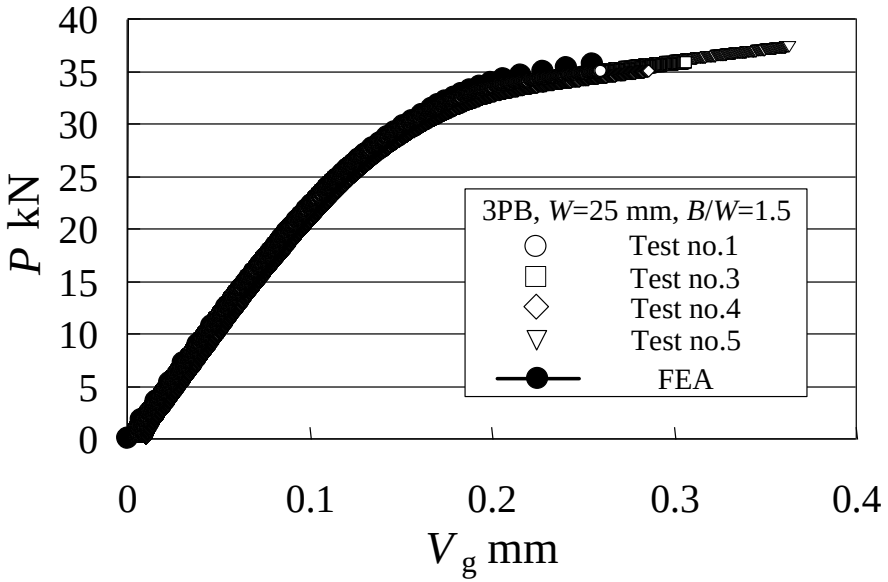

(d) $B/W = 1.5$

Fig. 12 Comparison of P-V diagrams determined by FEA and experiments

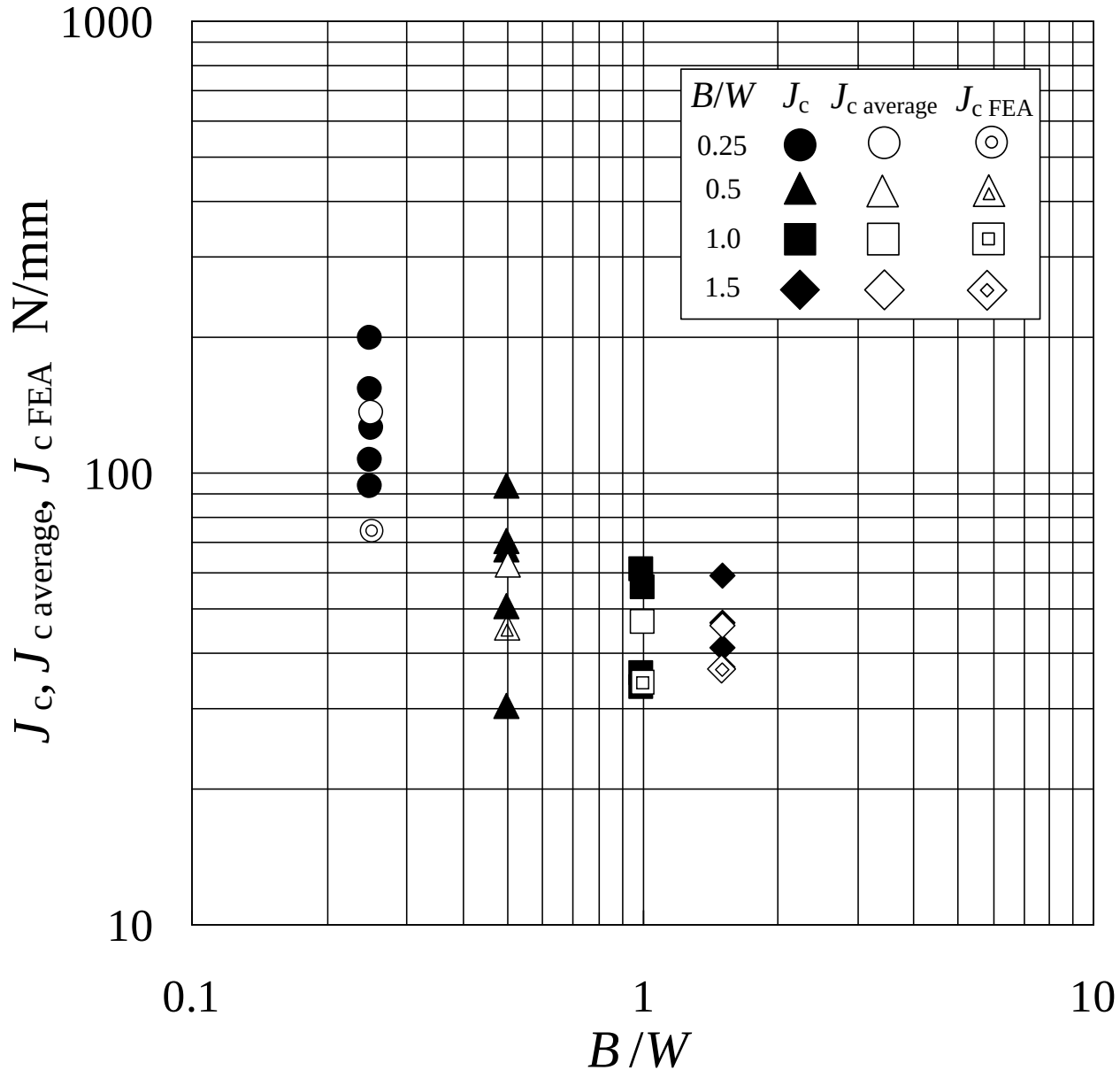

Fig. 13 Comparison of $J_{c\,FEA}$ and J_c for the non-standard 3PB specimens

(S55C, 20 ºC, W = 25 mm; $J_{c\,FEA}$ was obtained for average fracture load P_c in Table 4)

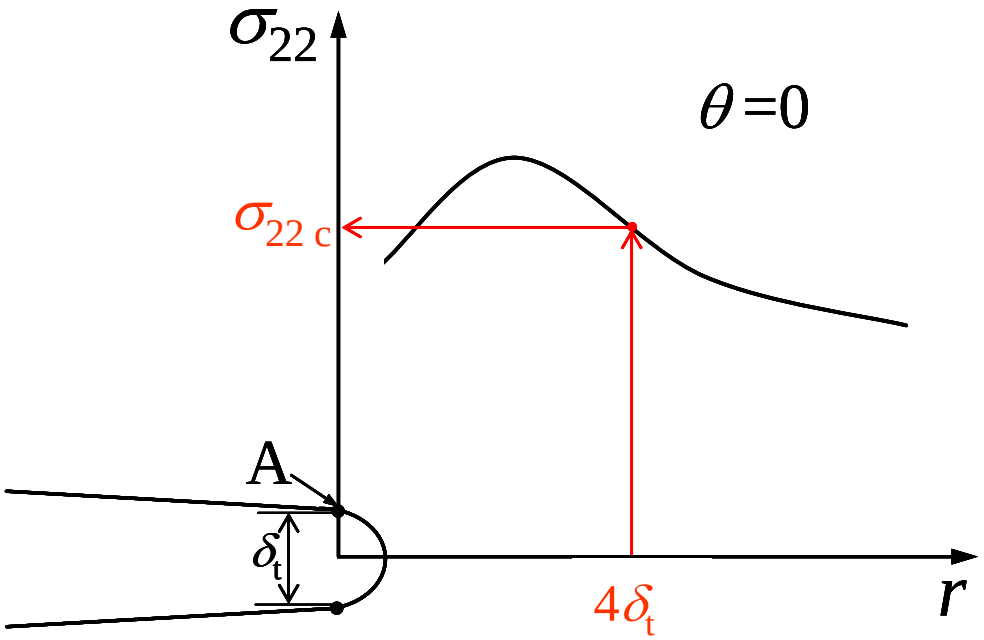

Fig. 14 “Planar” failure criterion [24]

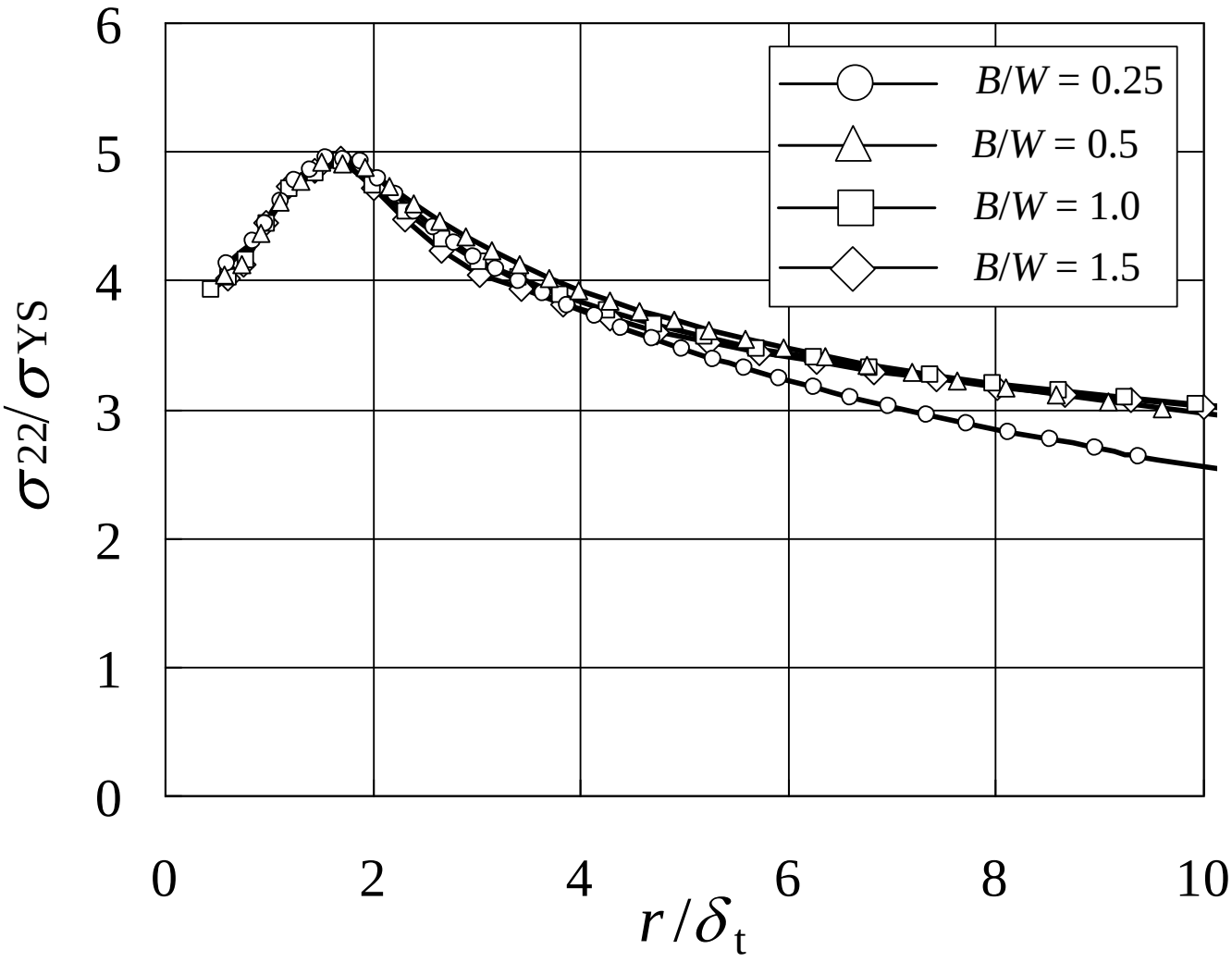

Fig. 15 Crack opening stress distribution for the non-standard 3PB specimen at fracture load P_c

(S55C, W = 25 mm, a/W = 0.5, specimen mid-plane, θ = 0)

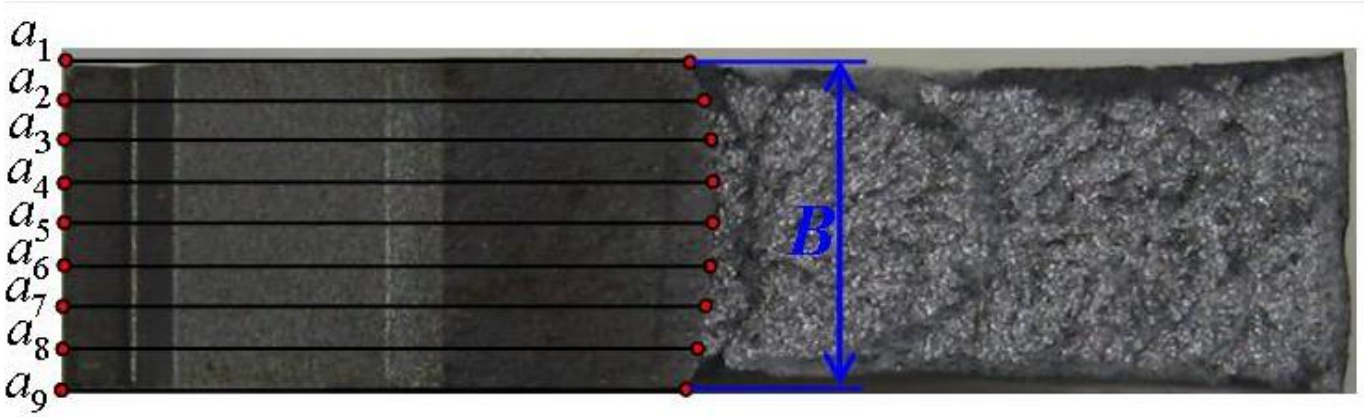

Fig. 16 Distributed crack length for B/W = 0.25 (specimen id 4)

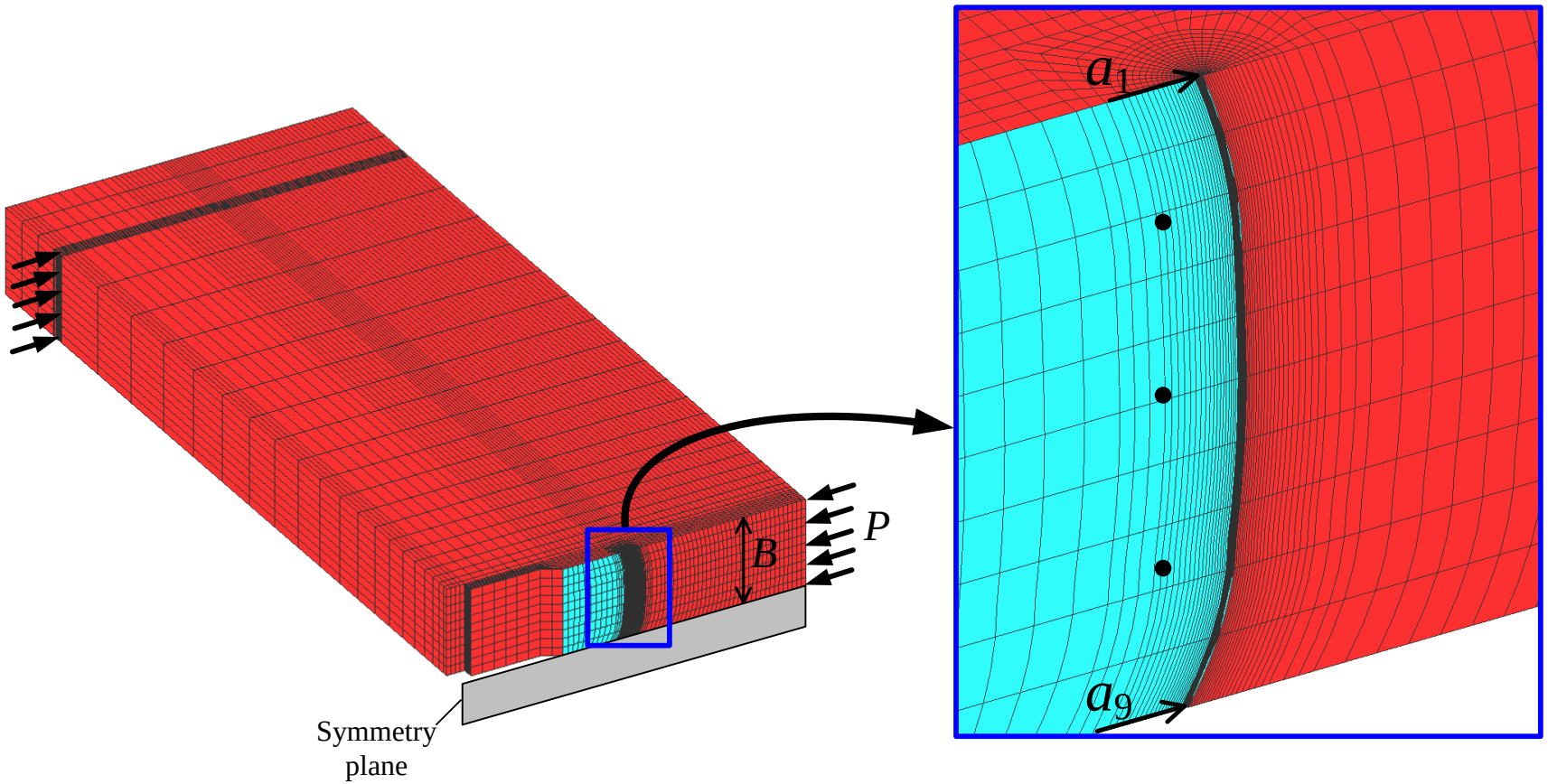

Fig. 17 Large-strain, elastic-plastic FEA model for $B/W = 0.25$ (distributed crack length)

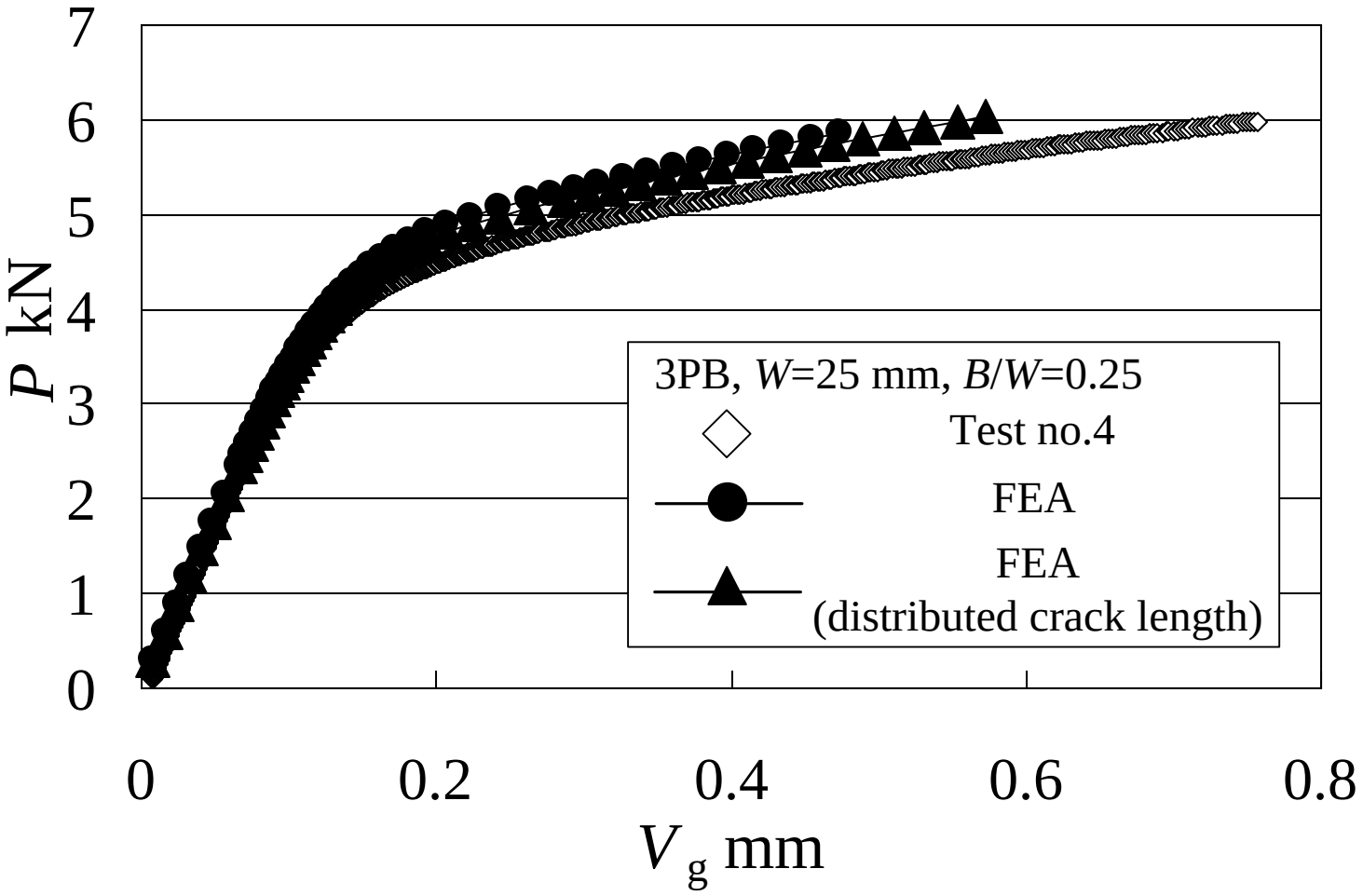

Fig. 18 Comparison of P-V diagrams determined by FEA (distributed crack length) and experiments

A Failure Criterion to Explain the Test Specimen Thickness Effect on Fracture Toughness in the Transition Temperature Region

Toshiyuki MESHII [a]*, Kai LU [b] and Ryota TAKAMURA[b]

[a] Faculty of Engineering, University of Fukui, 3-9-1 Bunkyo, Fukui, Fukui, JAPAN.

[b] Graduate Student, Graduate School of Engineering, University of Fukui, 3-9-1 Bunkyo, Fukui, Fukui, JAPAN.

*Correspondent, E-mail: meshii@u-fukui.ac.jp, FAX : +81-776-27-9764

Abstract

This paper considered the test specimen thickness (TST) effect on the fracture toughness of a material J_c in the transition temperature region for 3 point bending (3PB) specimens. Fracture toughness tests and elastic-plastic finite element analyses (FEA) with non-standard test specimens, which are non-standard because the specimen thickness-to-width ratio B/W was varied in the range of 0.25 to 1.5, were conducted. Based on these tests and the FEA results, it was demonstrated that the "planar" ($4\,\delta_t$, σ_{22c}) failure criterion—which states that cleavage fracture after significant plastic deformation occurs when the crack opening stress σ_{22} at a distance from the crack-tip that is equal to 4 times the crack-tip opening displacement δ_t exceeds a critical value σ_{22c}—was verified to effectively explain the TST effect. This ($4\delta_t$, σ_{22c}) criterion also successfully predicted the tendency of J_c to saturate to some bounding value for B/W=1.0. This tendency was similar to that of the T_{33}-stress, which is the out-of-plane elastic crack-tip constraint parameter. Because the ($4\delta_t$, σ_{22c}) criterion could predict the TST effect on J_c and because the criterion could predict the bounded behavior of J_c for large B/W, the TST effect was concluded to be mainly mechanical in nature, which the weakest link model fails to predict. The mechanical cause of the TST effect on J_c was considered to be an out-of-plane crack-tip constraint, and one of its measures of magnitude is the T_{33}-stress.

Key words: Fracture mechanics; Constraint effect, Fracture toughness, Cleavage fracture, Transition temperature, Thickness effect, 3PB specimen.

1. Introduction

One of the difficulties in determining the cleavage fracture toughness J_c of a material over the ductile-to-brittle transition (DBT) temperature region, which is important in the assessment of aging steel structures and reactor pressure vessels, is that test specimen thickness (TST) has an effect on J_c, even though standardized test specimens are used [1]. The two most physically logical effects, in general, are the statistically weakest link size effect and the loss of crack-tip constraint, that is, the effect caused by the loss of stress triaxiality [2]. The weakest link size effect should affect only brittle fracture, whereas the loss of constraint should affect both ductile and brittle fracture. Both criteria lead to increasing toughness with decreasing TST. Another point of view is that the former criterion considers the TST effect on J_c to be a material issue and the latter to be a mechanical issue.

This effect of TST on J_c, described as $J_c \propto B^{-1/2}$ ($B \equiv$ TST) by Wallin [2], was reproduced by Dodds et al. [3] based on the weakest link model. ASTM E1921 [4] has adopted parts of this criterion, and it seems to be widely accepted. However, as Dodds et al. [3] admit, "fracture toughness does not decrease indefinitely with thickness."

The crack-tip constraint approach to the TST effect on J_c assumes that the effect is a result of the out-of-plane crack-tip constraint. Guo [5, 6] proposed a parameter $T_z = \sigma_{33}/(\sigma_{11}+\sigma_{22})$ to measure the magnitude of the out-of-plane crack-tip constraint, and has been extensively working with co-workers to express the crack-tip stress field with a stress intensity factor (SIF) K or J-T_{11}-T_z [6-13]. Niemitz et al. [14] instead applied a J-Q-T_z approach to explain the difference in J_c. Whether explicitly expressed or not, Gao [15], Wang et al. [16-20], and Fernández-Sáez and Fernández-Canteli et al. [21] have focused their attention on the out-of-plane T-stress, T_{33}, as a measure of the out-of-plane crack-tip constraint. Based on this general methodology to express the magnitude of the 3D (including out-of-plane) crack-tip constraint, one of the authors [22] assumed that the TST effect on J_c was mechanical in nature and conducted fracture toughness tests and elastic-plastic finite element analyses (FEA) with non-standard compact-tension (CT) test specimens, using specimen thickness-to-width ratios, B/W, of 0.25, 0.4 and 0.5. The planar configuration was identical for the three cases and it complied with ASTM E399 [23] for W = 25 mm (these three types of test specimens are designated as non-standard test specimens). The key idea of this non-standard CT specimen was that the normalized planar parameter, $\beta_{11} = (\pi a)^{1/2}T_{11}/K$ (a = crack depth), is kept nearly constant, but the out-of-plane parameter, $\beta_{33} = (\pi a)^{1/2}T_{33}/K$, significantly changes for B/W. They successfully correlated the TST effect with a mechanical parameter as $J_c \propto |T_{33}|^{1/2}$ for 0.55% carbon steel JIS S55C in the DBT temperature region. The result was accepted as evidence that the TST effect on J_c is mechanical in nature, and the TST effect can be quantitatively described by some failure criterion independent of the specimen structure.

In this paper, as an extension of our previous work [22], the TST effect on J_c for a non-standard 3 point bending (3PB) specimen was studied to show that this effect is mechanical in nature. For this

purpose, fracture toughness tests with non-standard 3PB specimens were conducted for 0.55% carbon steel JIS S55C, and the TST effect was reproduced by running a large-strain, elastic-plastic FEA. Finally, it was demonstrated that the "planar" failure criterion proposed by Dodds et al. [24], i.e., that the "crack opening stress σ_{22c} together with the distance from the crack-tip which equals 4 times the crack-tip opening displacement δ_t," effectively explained the TST effect.

2. Fracture Toughness Test

2.1. Design of the non-standard 3PB specimens

It is well known that the widely accepted ASTM E1921 [4] (or E399 [23]) standard 3PB specimen (Fig. 1(a)) has a proportionally specified configuration based on its width W; i.e., the standard thickness-to-width ratio B/W is specified as 0.5 and the target crack depth-to-width ratio a/W is specified as 0.5. Under this specification, the normalized planar T-stress β_{11} (k = 1 in Eq. (1)) evaluated at the specimen mid-plane is approximately constant for W and, thus, for B. The starting point of our research was the recognition that if β_{11} represents the magnitude of the crack-tip constraint, then the TST effect on J_c observed for the standard 3PB specimens is independent of the crack-tip constraint. The volume of the specimen changes in proportion to B^3. When viewed in this manner, the explanation of the TST effect on J_c by the weakest link model, not by the loss of crack-tip constraint, is logical.

$$\beta_{kk} = T_{kk}\sqrt{\pi a}/K_{\mathrm{I}} \quad (k = 1 \text{or} 3)$$

where

$$\begin{Bmatrix} \sigma_{11} \\ \sigma_{22} \\ \sigma_{33} \\ \tau_{12} \\ \tau_{23} \\ \tau_{31} \end{Bmatrix} = \frac{K_{\mathrm{I}}}{\sqrt{2\pi r}} \begin{Bmatrix} \cos\frac{\theta}{2}\left(1-\sin\frac{\theta}{2}\sin\frac{3\theta}{2}\right) \\ \cos\frac{\theta}{2}\left(1+\sin\frac{\theta}{2}\sin\frac{3\theta}{2}\right) \\ 2\nu\cos\frac{\theta}{2} \\ \sin\frac{\theta}{2}\cos\frac{\theta}{2}\cos\frac{3\theta}{2} \\ 0 \\ 0 \end{Bmatrix} + \begin{Bmatrix} T_{11} \\ 0 \\ T_{33} \\ 0 \\ 0 \\ 0 \end{Bmatrix} \tag{1}$$

$$T_{33} = E\varepsilon_{33} + \nu T_{11} \tag{2}$$

The key idea in the design of the non-standard 3PB specimens for different Bs was to design the planar configuration to be in accordance with the ASTM E1921 (i.e., W = const.) but to change B/W to realize specimens with different thickness. With this design, it was expected that β_{11} would remain approximately constant but, because $|\varepsilon_{33}|$ in Eq. (2) decreases with increasing B, there would be a

significant change in β_{33} at the specimen mid-plane where the cleavage fracture initiates. Here, E and ν in Eq. (2) are the material's Young's modulus and Poisson's ratio, respectively.

If β_{33} represents the out-of-plane crack-tip constraint and the TST effect on J_c (TST effect) is observed for this non-standard 3PB specimen, then the out-of-plane crack-tip constraint might be a candidate to explain the TST effect. If J_c shows a saturation tendency with increasing B for this non-standard 3PB specimen and β_{33} also shows a similar tendency for an identical B, then the TST effect is likely to be dominated by the out-of-plane crack-tip constraint.

In the following, an elastic FEA for the non-standard 3PB specimen with W = 25 mm (Fig. 3) was run for various B/Ws to determine B such that β_{33} at the specimen mid-plane saturated. The typical FEA model used in elastic analysis of the 3PB specimen is shown in Fig. 4. The crack length a was prescribed as a/W = 0.5 for all cases. One-quarter of the structure was analyzed, making use of symmetry (Fig. 4 (a)). Twenty-node hexahedral meshes were used. For all cases, the crack-tip was modeled by singular elements, whose size was Δl, and twenty equivalent rows of meshes were spaced inside the crack tube with radius R_s = 0.4 mm (Fig. 4 (b)). The details for the generated mesh are summarized in Table 1. The Young's modulus, E = 206 GPa, and Poisson's ratio, ν = 0.3, were used in all cases. WARP3D [25] was used as the FEA solver.

The SIF was evaluated by applying the domain integral method [26] to the FEA results. T_{11} was obtained by applying the domain integral [26] and interaction integral [27] methods to the FEA results. These methods for calculating various T_{11} solutions have been used widely in the past [12, 18-20]. T_{33} was evaluated from Eq. (2). The results at the specimen mid-plane are summarized in the normalized form as K/K_0, $\beta_{kk} = T_{kk}(\pi a)^{1/2}/K_0$ (k = 1, 3) in Fig. 5, in which K_0 is the nominal SIF calculated from the following equation in ASTM E1921 [4], corresponding to the load used for the calculation.

$$K = \frac{PS}{BW^{3/2}} f\left(\frac{a}{W}\right) \qquad (3)$$

Here, $S = 4W$ is the support span, and f is a function of a/W that is given in the standard. Attention was focused upon the values at the mid-plane because the cleavage fracture is expected to initiate at the specimen mid-plane.

According to Fig. 5, the mid-plane K was not affected by B/W, as expected, and was close to the nominal 2D SIF K_0. The normalized T_{11}, where $\beta_{11} = T_{11}(\pi a)^{1/2}/K_0$, was positive, showing negligible dependence on B/W. The in-plane parameters at the specimen thickness center showed a slight dependence on B/W, as expected.

The dotted line represents $\nu\beta_{11}$, which denotes the case for $B/W \rightarrow \infty$ and $\varepsilon_{33} \rightarrow 0$, i.e., $T_{33} \rightarrow \nu T_{11}$ calculated from Eq. (2). The normalized T_{33}, where $\beta_{33} = T_{33}(\pi a)^{1/2}/K_0$, showed a strong dependence on B/W. β_{33} was negative for $B/W < 1.5$, very close to 0 for $B/W = 1.5$, positive for $B/W > 1.5$ and approached $\nu\beta_{11}$ with increasing B/W. Because a negative T-stress corresponds to a loss in

crack-tip constraint [28], it appears that T_{33} represents the well-known tendency for a larger out-of-plane crack-tip constraint to be expected for thick test specimens. If β_{33} represents the out-of-plane crack-tip constraint and if J_c has some bounding value for B due to the bounding nature of the crack-tip constraint for large B, deviation from the relationship $J_c \propto B^{-1/2}$ was expected to be observed for the non-standard 3PB specimen of $B/W \geq 1.5$. Because the magnitude of the positive T-stress is known to be insensitive to the crack-tip constraint [28] and because the load capacity of the testing machines is limited, fracture toughness tests for non-standard 3PB specimens with B/W = 0.25, 0.5, 1.0 and 1.5 were conducted.

2.2. Fracture toughness tests with the non-standard 3PB specimens

2.2.1. Material

The tested material was 0.55% carbon steel JIS S55C, which is known to be in the transition temperature region at room temperature. From the Charpy test results shown in Fig. 6, the fracture toughness test temperature was chosen to be 20 ^{o}C. The material was quenched at 850 ^{o}C and tempered at 650 ^{o}C. Chemical composition and mechanical properties of the heat-treated specimens are summarized in Tables 2 and 3, respectively. Two tensile tests were conducted in accordance with JIS Z2241 [29]. The loading rates of the tensile tests were 10 MPa/sec below 0.2% strain and 30 %/min (measured at the gage length) above 0.2%, which satisfies the JIS Z2241 [29] requirements of 3-30 MPa/sec below 0.2% strain and 20-50% /min (measured at the gage length) above 0.2%. The tensile test temperature was 20 ^{o}C.

2.2.2. Test specimens

As described in 2.1, the planar test specimen configurations were designed in accordance with ASTM E1921 [4] for width W = 25 mm, i.e., W was prescribed to be 25 mm for all specimens. In addition to the standard ASTM thickness-to-width ratio, B/W = 0.5, specimens with B/W = 0.25, 1.0, and 1.5 were prepared. After inserting a fatigue crack into the specimen, the crack length a satisfied ASTM's requirement of a/W = 0.45-0.55; the crack length was in the range of 0.49 to 0.51. Fatigue precrack was inserted at 20 ^{o}C with loads corresponding to K_{max} = 20 and 19 MPam$^{1/2}$ for the 1st and 2nd stages, respectively, which satisfied the requirement of the standard 25 and 20 MPam$^{1/2}$. Fatigue crack growth was monitored by clip gage. Five tests were conducted for each test specimen geometry.

2.2.3. Test results

The fracture toughness test was conducted in accordance with ASTM E1921 [4]. The loading rate was controlled to be 1.1 MPam$^{1/2}$/s, which is very small compared to the specification of ≤ 2.0 MPam$^{1/2}$/s. The test specimen temperature was maintained to be in the range of 20 ± 1 ^{o}C for

30/(25/B) minutes for B/W = 1.0 and 1.5, according to the standard. The hold time for the other cases of B/W = 0.25 and 0.5 was 30 minutes, which is longer than the standard hold time.

Typical fracture surfaces observed at the mid-plane for specimens of B/W = 0.25, 0.5 and 1.0 are shown in Fig. 8. It is clearly seen from Fig. 8 that cleavage fracture after plastic deformation was observed for all specimens with different B/Ws. Although not shown in this manuscript, a similar fractograph was observed for the case of B/W = 1.5. The difference observed in these three B/Ws was that the distance between the fatigue precrack and the river pattern decreased as B/W increased, corresponding to a decrease in the plastic zone.

Test results are summarized in Table 4 and Fig. 9. K_c in the table was obtained from Eq. (3) and is the SIF K corresponding to the maximum load, P_c. K_{Jc} in the table is the fracture toughness in terms of the SIF, defined as $K_{Jc} = [EJ_c/(1-\nu^2)]^{1/2}$, as specified in ASTM E1921 [4]. μ and Σ are the average and standard deviation of each value, respectively. $2\Sigma/\mu$ % is a reference value intended to represent the magnitude of data scatter.

It is seen from Table 4 that $2\Sigma/\mu$ of K_{Jc} were in the range of 20.7 to 39.9 % for all the specimens. Considering that the guideline for $2\Sigma/\mu$ given in ASTM E1921 for K_{Jc} is $56(1-20/\mu)$ % and was in the range of 45.0 to 49.5 % for the data in Table 4, it was concluded that the scatter in the K_{Jc} data summarized in the table is acceptable. In addition, if the datam for specimen number 1 with B/W = 0.5 is excluded, it can be said that a very small scatter in K_{Jc} was realized from the current test data.

One interesting fact was that the change in K_c, the SIF for the fracture load P_c, with B/W was very small, though a significant change in J_c was observed. The average K_c for each B/W was in the range of 61.1 to 64.0 MPam$^{1/2}$.

From Fig. 9, the TST effect on J_c was clearly observed for the non-standard 3PB specimens. The raw J_c tended to decrease as B/W increased in the range of 0.25 to 1.0 and seemed to saturate to a value around 46 N/mm for B/W = 1.5. If the relationship between the average values of J_c and B/W were fitted to $J_c \propto (B/W)^{-n}$, then n was large as 1 in the range of B/W = 0.25 to 0.5, decreased to 0.5 in the range of B/W = 0.5 to 1.0 and was almost 0 in range of B/W = 1.0 to 1.5; it was thus concluded that J_c was bounded for B/W = 1.5, on the point of the average of J_c.

In summary, by changing β_{33} for B/W of the non-standard 3PB, J_c displayed bounded behavior for large B and, thus, deviation from the relationship $J_c \propto B^{-1/2}$ was observed. This result was as expected under the assumptions that β_{33} represents the out-of-plane crack-tip constraint and that J_c is affected by this crack-tip constraint.

3. Failure Criterion to Account for the TST Effect on J_c

3. 1 Reproduction of the experiments with a large-strain, elastic-plastic FEA

First, a large-strain, elastic-plastic FEA for the non-standard 3PB test specimens was conducted to validate the assumption that the TST effect on J_c is mechanical in nature by reproducing the depicted experimental results without assuming the existence of micro-cracks in the material. After the assumption was validated, a failure criterion to explain the TST effect on J_c was proposed.

The FEA model used in the elastic-plastic analysis of the 3PB specimen is fundamentally similar with the model used for the elastic analysis shown in Fig. 4. The width W was 25 mm and the crack length a was 12.5 mm (a/W = 0.5) for all the models. One-quarter of the structure was analyzed to make use of the symmetry of the specimen as shown in Fig. 10(a). Twenty node hexahedral meshes were used. To run this large-strain elastic-plastic analysis, an initial blunted notch ρ was inserted at the crack-tip as shown in Fig. 10(b). Twenty rows of meshes were spaced around the notch and inside crack tube R_s = 0.8 mm. Equivalent elements were spaced in thickness direction. The details for the generated mesh are summarized in Table 5. In this case, ρ was validated by the relationship between the crack-tip opening displacement δ_t measured at node A in Fig. 10(b); in particular, δ_t/ρ was greater than 10. McMeeking and Parks [30] suggested that δ_t/ρ should be greater than 5 to ensure that the results would not be affected by the initial blunt notch. In addition, the FEA results were considered sufficiently accurate with very refined meshes because the blunted crack tip was always defined by fairly regularly spaced nodes and the region around a crack tip up to a distance of a few crack-tip openings was always composed of elements that were very small compared to δ_t.

WARP3D [25] was used for the large-strain, elastic-plastic analysis. The material behavior was assumed to be governed by the J2–incremental theory of plasticity, the isotropic hardening rule and the Prandtl–Reuss flow theory. The Newton–Raphson iterative method was used for the nonlinear convergence. The Young's modulus E = 206 GPa and Poisson's ratio ν = 0.3 were used for all cases. Because S55C is a material with yield drop, the total true stress-total true strain curve in the range up to the true fracture stress obtained from the two tensile tests was approximated as a piecewise-linear stress-strain curve, as shown in Fig. 11. Note that WARP3D [25] allows this kind of material modeling.

The maximum load for each B/W was selected as the average fracture load P_c obtained from the experiments, summarized in Table 4. Load P vs. crack-mouth opening displacement V_g curves (P-V diagrams) obtained from the FEA for each specimen type is compared with the experimental results in Fig. 12. J at the maximum load P_c was obtained from these FEA P-V diagrams in accordance with the ASTM E1921 [4] and designated as $J_{c\ FEA}$. This $J_{c\ FEA}$ was compared with the experimental results in Fig. 13.

It is seen in Fig. 12 that the large-strain, elastic-plastic FEA accurately reproduced the P-V diagrams observed from experiments, though a noticeable discrepancy was shown for the case B/W

= 0.25. The source of this discrepancy is examined in the Discussion. Although the fracture load P_c showed some scatter and the clip gage displacement at fracture also showed scatter, experimental P-V data for all the specimens were close to the curve drawn from the FEA results.

From Fig. 13, it is seen that $J_{c\ FEA}$ clearly reproduced the TST effect on J_c observed by the experiments. This was natural, because $J_{c\ FEA}$ was evaluated from the P-V diagrams that were confirmed to be fairly close to the experimental data. In addition, $J_{c\ FEA}$ displayed bounded behavior for large *B*.

In summary, by assuming the average fracture load P_c for each *B*/*W* of the non-standard 3PB specimens, *J* obtained from large strain FEA results at this P_c reproduced the TST effect on J_c observed from experiments. Because this large strain FEA did not assume existence of micro-cracks, but β_{33} was designed to be changed with the *B*/*W* of the non-standard 3PB specimens, TST effect on J_c seemed to be mechanical in nature, under the assumptions that β_{33} is to represent the out-of-plane crack-tip constraint.

3. 2 Failure criterion to explain the TST effect on J_c

If the TST effect on J_c is mechanical in nature, it was thought that a failure criterion applicable to large-strain, elastic-plastic FEA results that explains the TST effect on J_c might exist. The key idea for this criterion was that K_c, which is the SIF calculated from the fracture load P_c and the specimen size, was slightly dependent on TST, though J_c was significantly dependent, as shown in Table 4. The hypothesis was that the (in-plane) crack opening stress σ_{22} distribution for each specimen type at the critical load P_c may be similar, even though J_c shows noticeable effects from a change in *B*/*W*. This is because a change in *B*/*W* causes a negligible change in T_{11}. Thus, the "planar" failure criterion, similar to the one that Dodds et al. [24] applied to explain the J_c-dependence on the test specimen crack depth (as shown in Fig. 14), might be applied to explain the out-of-plane TST effect on J_c. The critical values of this criterion ($4\delta_t$, σ_{22c}), in which δ_t denotes the CTOD (crack-tip opening displacement) and σ_{22c} denotes the crack-opening stress, was evaluated as a first step.

The distribution of the crack opening stress σ_{22} ($\theta = 0$) at the specimen mid-plane ahead of the crack-tip with the fracture load P_c for all *B*/*W*s are shown in Fig. 15. σ_{YS} in the figure is the true yield stress. σ_{22} ($\theta = 0$) for all *B*/*W*s showed a similar tendency; specifically, σ_{22} attained a maximum value approximately equal to $5\sigma_{YS}$ at approximately $2\delta_t$. This maximum was comparable with that for a material with a hardening component of 5 at plane-strain, approximately equal to $5\sigma_{YS}$ [31].

The ($4\delta_t$, σ_{22c}) corresponding to the mid-plane $J_{c\ FEA}$ for each *B*/*W* calculated in 3.1 is summarized in Table 6. It is seen from Table 6 that the critical stress σ_{22c} at $4\delta_t$ on the crack plane ($\theta = 0$) was very close for all *B*/*W*s in an engineering sense, though $J_{c\ FEA}$ for each *B*/*W* showed significant variation. The $J_{c\ FEA}$ at the mid-plane of the specimen was focused upon because cleavage fracture initiated at the specimen mid-plane. Because the σ_{22c} values for all the *B*/*W*s were very close

at the fracture load for each P_c and J_{cFEA} at P_c reproduced the TST effect on J_c, it was concluded that the ($4\delta_t$, σ_{22c}) criterion successfully explained the TST effect on J_c.

In summary, the "planar" failure criterion ($4\delta_t$, σ_{22c}), which was applied to explain the crack depth dependence on J_c by Dodds et al. [24], successfully reproduced the TST effect on J_c that is observed in fracture toughness tests, under the assumption that the TST effect on J_c is mechanical in nature.

4. Discussion

In this work, the TST effect on J_c observed for 0.55% carbon steel S55C in the transition temperature range was reproduced by large-strain FEA results. Neither the micro-crack density distribution nor the weakest link model was assumed to apply to the material, as Dodds et al. did to deduce the relationship $J_c \propto B^{-1/2}$ [3]. The idea to change the crack-tip volume proportionally to the specimen thickness is common for non-standard specimens and the Dodds et al. framework. In addition, the "planar" failure criterion successfully explained the TST effect. Thus, it seems that the mechanical nature of the TST effect on J_c cannot be denied. At least, the bounded behavior of J_c with increasing B seems to be dominated by the mechanical nature. One of the candidates for this mechanical cause is the change in the out-of-plane crack-tip constraint. The only assumption applied in this study was that the fracture initiates at the specimen mid-plane.

In Fig. 12 (a), a noticeable discrepancy was shown for the P-V diagram of B/W = 0.25 obtained from both the experiments and FEA. The FEA was performed by assuming the crack length to be uniform in thickness direction and set as a/W = 0.5 (Fig. 10 (a)). However, after the fatigue pre-crack procedure, the crack length was, in fact, distributed along the thickness direction, especially for B/W = 0.25, as shown in Fig. 16 and Table 7. Thus, a large-strain, elastic-plastic FEA was performed for a case of B/W = 0.25, reflecting the fatigue crack length distribution for specimen id 4 as shown in Fig. 17.

The P-V diagram was compared with both the experiment and previous FEA results as shown in Fig. 18. It is seen from Fig. 18 that the P-V diagram from the FEA with a distributed length is closer to the experimental results. $J_{c\,FEA}$ obtained from the current P-V diagram increased to 90.3 N/mm, which corresponds to a 21.4 % increase from the uniform crack model 74.4 N/mm. This $J_{c\,FEA}$ for specimen id 4 became comparable to the minimum 93.4 N/mm of the experimental value, but is still smaller than the experimental result of 125.0 N/mm. Therefore, through-thickness crack length distribution was one noticeable source of discrepancy between J_{cFEA} and J_c for relatively thin specimens.

There might be an opinion that the quantity of the micro-cracks might have contributed in the discrepancy still remaining between $J_{c\,FEA}$ and J_c for this B/W. However, this discrepancy between $J_{c\,FEA}$ and J_c here is due to the discrepancy of P-V diagrams for FEA and experiments as shown in Fig. 18. Though not numerically verified, it seems difficult that the micro-crack density significantly affects a gross deformation, such as the P-V diagram. Therefore, the calculated J value from the P-V diagram seems also not to be significantly affected by micro-cracks.

5. Conclusions

This study investigated the TST effect on the fracture toughness J_c of a material in the transition temperature region for 3PB specimens. Fracture toughness tests and elastic-plastic FEA on non-standard test specimens, with thickness-to-width ratios B/W of 0.25, 0.5, 1.0 and 1.5, were conducted for 0.55% carbon steel. The conclusions are as follows.

- The TST effect on J_c and bounded behavior of J_c for increasing specimen B/W was observed with the non-standard 3PB specimen, as intended.
- Large-strain, elastic-plastic FEA reproduced the behavior observed in the experiments.
- The ($4\delta_t$, σ_{22c}) criterion effectively explained the TST effect and the bounded behavior of J_c.
- The bounded behavior of J_c for increasing B seems to be dominated by mechanical causes. One of the candidates for this mechanical cause is the change in out-of-plane crack-tip constraint.

Acknowledgement

Part of this work is supported by JSPS KAKENHI Grant Number 2456103. Their support is greatly appreciated.

List of figures

List of tables

References

[1] Petti JP, Dodds RH. Coupling of the Weibull stress model and macroscale models to predict cleavage fracture. Engineering Fracture Mechanics. 2004;71:2079-103.

[2] Wallin K. The size effect in K_{IC} results. Engineering Fracture Mechanics. 1985;22:149-63.

[3] Anderson TL, Stienstra D, Dodds RH. A Theoretical Framework for Addressing Fracture in the Ductile-Brittle Transition Region. In: Landes JD, McCabe DE, Boulet JAM, editors. STP1207, Fracture Mechanics: 24th Volume. Philadelphia: American Society for Testing and Materials; 1994. p. 186-214.

[4] ASTM. E1921-10 Standard Test Method for Determination of Reference Temperature, T_o, for Ferritic Steels in the Transition Range. Annual Book of ASTM Standards. Philadelphia PA: American Society for Testing and Materials; 2010.

[5] Guo W. Elastoplastic three dimensional crack border field--I. Singular structure of the field. Engineering Fracture Mechanics. 1993;46:93-104.

[6] Guo W. Elastoplastic three dimensional crack border field--II. Asymptotic solution for the field. Engineering Fracture Mechanics. 1993;46:105-13.

[7] Zhang B, Guo W. T_z constraints of semi-elliptical surface cracks in elastic plates subjected to uniform tension loading. International Journal of Fracture. 2005;131:173-87.

[8] Zhao J, Guo W, She C, Meng B. Three dimensional K-T_z stress fields around the embedded center elliptical crack front in elastic plates. Acta Mechanica Sinica. 2006;22:148-55.

[9] Zhao J, Guo W, She C. The in-plane and out-of-plane stress constraint factors and K-T-T_z description of stress fields near the border of a quarter-elliptical corner crack. Fatigue & Fracture of Engineering Materials & Structures. 2007;30:673-81.

[10] She C, Guo W. The out-of-plane constraint of mixed-mode cracks in thin elastic plates. International journal of solids and structures. 2007;44:3021-34.

[11] Zhang B, Guo W. Three-dimensional stress state around quarter-elliptical corner cracks in elastic plates subjected to uniform tension loading. Engineering Fracture Mechanics. 2007;74:386-98.

[12] Zhao J, Guo W, She C. The in-plane and out-of-plane stress constraint factors and K-T-T_z description of stress field near the border of a semi-elliptical surface crack. International Journal of Fatigue. 2007;29:435-43.

[13] Zhao J, Guo W, She C. Three-parameter approach for elastic-plastic fracture of the semi-elliptical surface crack under tension. International Journal of Mechanical Sciences. 2008;50:1168-82.

[14] Neimitz A, Galkiewicz J. Fracture toughness of structural components: influence of constraint. International Journal of Pressure Vessels and Piping. 2006;83:42-54.

[15] Gao H. Variation of elastic T-stresses along slightly wavy 3D crack fronts. International Journal of Fracture. 1992;58:241-57.

[16] Wang X. Elastic T-stress solutions for semi-elliptical surface cracks in finite thickness plates. Engineering Fracture Mechanics. 2003;70:731-56.

[17] Wang X. Elastic T-stress solutions for penny-shaped cracks under tension and bending. Engineering Fracture Mechanics. 2004;71:2283-98.

[18] Lewis T, Wang X. The T-stress solutions for through-wall circumferential cracks in cylinders subjected to general loading conditions. Engineering Fracture Mechanics. 2008;75:3206-25.

[19] Wang X, Bell R. Elastic T-stress solutions for semi-elliptical surface cracks in finite thickness plates subject to non-uniform stress distributions. Engineering Fracture Mechanics. 2004;71:1477-96.

[20] Qu J, Wang X. Solutions of T-stresses for quarter-elliptical corner cracks in finite thickness plates subject to tension and bending. International Journal of Pressure Vessels and Piping. 2006;83:593-606.

[21] González-Albuixech VF, Giner E, Fernández-Sáez J, Fernández-Canteli A. Influence of the T_{33}-stress on the 3-D stress state around corner cracks in an elastic plate. Engineering Fracture Mechanics. 2011;78:412-27.

[22] Meshii T, Tanaka T. Experimental T_{33}-stress formulation of test specimen thickness effect on fracture toughness in the transition temperature region. Engineering Fracture Mechanics. 2010;77:867-77.

[23] ASTM. E399-05 Standard Test Method for Plane-Strain Fracture Toughness of Metallic Materials. Annual Book of ASTM Standards. Philadelphia PA: American Society for Testing and Materials; 2005.

[24] Dodds RH, Anderson TL, Kirk MT. A framework to correlate a/W ratio effects on elastic-plastic fracture toughness (J_c). International Journal of Fracture. 1991;48:1-22.

[25] Gullerud A, Koppenhoefer K, Roy Y, RoyChowdhury S, Walters M, Bichon B, et al. WARP3D Release 15 Manual. Civil Engineering, Report No UIUCENG-95-2012, University of Illinois at Urbana-Champaign. 2004.

[26] Li FZ, Shih CF, Needleman A. A comparison of methods for calculating energy release rates. Engineering Fracture Mechanics. 1985;21:405-21.

[27] Nakamura T, Parks DM. Determination of elastic T-stress along three-dimensional crack fronts using an interaction integral. International journal of solids and structures. 1992;29:1597-611.

[28] Bilby BA, Cardew GE, Goldthorpe MR, Howard IC. A finite element investigation of the effect of specimen geometry on the fields of stress and strain at the tips of stationary cracks. Size Effects in Fracture. London: Mechanical Engineering Publications Limited; 1986. p. 37-46.

[29] JIS. Z2241 Method of tensile test for metallic materials. Tokyo: Japanese Industrial Standards Committee; 1998.

[30] McMeeking RM, Parks DM. On criteria for J-dominance of crack-tip fields in large-scale yielding. In: Landes John D, Begley JA, Clarke GA, editors. STP 668, Elastic-Plastic Fracture. Philadelphia, PA; USA: American Society for Testing and Materials; 1979. p. 120-38.

[31] McMeeking RM. Finite deformation analysis of crack-tip opening in elastic-plastic materials and implications for fracture. Journal of the Mechanics and Physics of Solids. 1977;25:357-81.